# Computing spectral densities in finite temperature field theory

Sangyong Jeon
*Physics Department FM-15, University of Washington, Seattle, Washington 98195*
(Received 25 August 1992)

Convenient Cutkosky-like diagrammatic rules for computing the spectral densities of arbitrary two-point correlation functions in finite temperature field theory are derived. The approach is based on an explicit analytic continuation of imaginary-time Feynman diagrams. The application of this method to the perturbative evaluation of transport coefficients is briefly discussed.

PACS number(s): 11.10.Ef

## I. INTRODUCTION

Linear response functions characterize the behavior of an equilibrium thermodynamic system when subjected to a small disturbance [1]. Important examples include shear and bulk viscosities, thermal or electric conductivities, and magnetic susceptibilities. Any response function may be expressed in terms of a spectral density defined, for any pair of operators $\hat{A}$ and $\hat{B}$, as

$$\rho_{AB}(\mathbf{k},\omega) \equiv \int d^3\mathbf{x}\, dt\, e^{-i\mathbf{k}\cdot\mathbf{x}+i\omega t} \langle[\hat{A}(\mathbf{x},t),\hat{B}(0)]\rangle \ . \quad (1.1)$$

For example, the static shear viscosity may be shown to equal [2,3]

$$\eta = i\int d^3\mathbf{x} \int_{-\infty}^{0} dt \int_{-\infty}^{t} dt' \ \langle[\hat{\pi}_{kl}(0),\hat{\pi}_{kl}(\mathbf{x},t')]\rangle$$
$$= \frac{1}{2}\frac{d}{d\omega}\rho_{\pi\pi}(0,\omega)|_{\omega=0} \ , \quad (1.2)$$

where $\hat{\pi}_{kl}(\mathbf{x},t)$ is the traceless part of the spatial stress tensor. For instance, in a scalar field theory $\hat{\pi}_{kl} = \partial_k\hat{\phi}\,\partial_l\hat{\phi} - \frac{1}{3}\delta_{kl}\partial_m\hat{\phi}\,\partial_m\hat{\phi}$.

All transport coefficients are determined by the low frequency, zero momentum limit of the spectral density of the appropriate composite operators, as in Eq. (1.2). The purpose of this paper is to examine the perturbative calculation of composite operator spectral densities in this limit. For simplicity, the calculation of the spectral density of the correlation function $\langle[\hat{\phi}^2(\mathbf{x},t),\hat{\phi}^2(0)]\rangle$ in a real scalar $\lambda\phi^4$ theory is discussed. At zero momentum, this correlation function has analytic structure similar to the spectral density of the stress tensor correlation function, but avoids inessential notational complications.

Despite the simplicity of the definition (1.1), spectral densities are not easy quantities to evaluate perturbatively at nonzero temperature. Appropriate calculational rules for the spectral density of general operators are derived in the first part of this paper, starting from the standard imaginary-time diagrammatic rules for a relativistic field theory. Then, the application of these rules to the calculation of the spectral density $\langle[\hat{\phi}^2(\mathbf{x},t),\hat{\phi}^2(0)]\rangle$ is examined. Individual Feynman diagrams, computed with free thermal propagators, are shown to produce severe infrared divergences. These divergences reflect a nonuniformity in the low frequency and weak coupling limit. When calculated correctly, the would-be infrared divergences are cut off by the thermal lifetime of the particles. However, even after accounting for the finite single particle lifetime, an infinite number of diagrams must still be summed to obtain the correct leading-order low-frequency behavior.[1]

Previously, several authors [5–7] have discussed rules for the calculation of the imaginary part of a given diagram within the real-time formalism. This work, when combined with Refs. [8,9], yields a set of rules for the evaluation of the spectral densities of elementary fields equivalent to the rules derived here.[2] The derivation given below, based on the imaginary-time formalism, is entirely self-contained and easily permits inclusion of the necessary self-energy resummations. Whether one prefers to begin with the real-time or imaginary-time formalism is ultimately a matter of taste, and cannot affect the final result.

This paper is organized as follows. In the remainder of the Introduction, the real-time formalism and imaginary-time approaches are briefly described. The calculation of imaginary-time correlation functions is reviewed in Sec. II. Section III shows how the process of analytic continuation and computation of the discontinuity can be carried out in a convenient form. (For nonrelativistic theories, a similar discussion of a portion of this approach may be found in Ref. [10].) In Sec. IV, it is shown how to incorporate the results of previous sections into a convenient set of diagrammatic rules. The resulting method is then applied in Sec. V to a simple example of the spectral density of the composite operator correlation function $\langle[\hat{\phi}^2(\mathbf{x},t),\hat{\phi}^2(0)]\rangle$ in a scalar $\lambda\phi^4$ theory. Appendix A discusses the symmetry properties of the spectral density and the implications of *CPT* invariance. For

[1]Similar summations must also be performed in nonrelativistic calculations of transport coefficients [4].

[2]The extension to arbitrary operators is a straightforward generalization of [8].

 

ease of the presentation, the body of this paper discusses theories with zero chemical potential and composite operators without time derivatives. Appendix B generalizes the treatment to operators involving time derivatives of the elementary field, and the generalization to nonzero chemical potential is presented in Appendix C.

The spectral density is the difference between the advanced and retarded correlation functions:

$$i\rho_{AB}(\mathbf{k},\omega) = \tilde{G}^{\rm adv}_{AB}(\mathbf{k},\omega) - \tilde{G}^{\rm ret}_{AB}(\mathbf{k},\omega) \; . \tag{1.3}$$

These correlation functions

$$\tilde{G}^{\rm adv,ret}_{AB}(\mathbf{k},\omega) \equiv \pm i \int d^3\mathbf{x}\, dt\, e^{-i\mathbf{k}\cdot\mathbf{x}+i\omega t}\, \theta(\pm t) \times \langle [\hat{A}(\mathbf{x},t), \hat{B}(0)] \rangle \tag{1.4}$$

have the spectral representation

$$\tilde{G}^{\rm adv,ret}_{AB}(\mathbf{k},\omega) = \int \frac{d\omega'}{2\pi} \, \frac{\rho_{AB}(\mathbf{k},\omega')}{\omega' - \omega \mp i\epsilon} \; , \tag{1.5}$$

with the upper sign referring to the advanced and the lower sign to the retarded function.

In the real-time formalism at nonzero temperature, the number of fields are doubled [11], and the retarded and advanced correlation functions can be expressed in terms of the time-ordered correlation function of the doubled fields [8,9]. The perturbative evaluation of any time-ordered correlation function, in the real-time formalism, requires using a matrix-valued propagator. For a scalar theory, this has the form [11]

$$\tilde{G}^F_0(k) = \begin{pmatrix} \Delta_{++}(k) & \Delta_{+-}(k) \\ \Delta_{-+}(k) & \Delta_{--}(k) \end{pmatrix} \; , \tag{1.6}$$

where

$$\Delta_{++}(k) = \Delta_{--}(k)^* = \frac{i}{k^2 + m^2 - i\epsilon} - \frac{2\pi}{e^{\beta|k_0|} - 1} \delta(k^2 + m^2) \tag{1.7}$$

and

$$\Delta_{+-}(k) = \Delta_{-+}(k) = \frac{e^{\beta|k_0|/2}}{e^{\beta|k_0|} - 1} \, 2\pi\delta(k^2 + m^2) \; . \tag{1.8}$$

This structure arises because the finite temperature, real-time correlation function necessarily involves time evolution operators propagating both forward and backward in time. To see this, note that in the interaction picture

$$\langle \mathcal{T}(\hat{A}(\mathbf{x},t)\hat{B}(0)) \rangle = \lim_{T\to\infty} {\rm Tr} \left[ \hat{U}_I(-i\beta - T, T)\, \mathcal{T}\Big( \hat{A}_I(\mathbf{x},t) \hat{B}_I(0) \hat{U}_I(T,-T) \Big)\, e^{-\beta \hat{H}_0} \right] \Big/ {\rm Tr}\, e^{-\beta \hat{H}} \; , \tag{1.9}$$

where the subscript $I$ signifies the interaction picture operators, $\hat{H}$ is the full Hamiltonian and $\hat{H}_0$ is the free Hamiltonian. To evaluate this perturbatively, one must expand both time evolution operators. The time evolution operator that propagates forward (from $-\infty$ to $+\infty$) generates ordinary time-ordered products, but the time evolution operator that propagates backward (from $+\infty$ to $-\infty - i\beta$) generates anti-time-ordered products. This difference cannot be avoided at finite temperature and is ultimately reflected in the different signs of $i\epsilon$ in $\Delta_{++}$ and $\Delta_{--}$. Only the $\Delta_{++}$ part of the propagator has the right structure to represent real particle propagation. The other elements of the matrix propagator model the heat bath and also serve to cancel unphysical singularities that would occur if only the $\Delta_{++}$ part of the propagator were used.

Alternatively, in the imaginary-time formalism, one may obtain the advanced and retarded two-point functions (and hence the spectral density) from the time-ordered imaginary-time correlation function,

$$G^E_{AB}(\mathbf{x},\tau) \equiv \langle \mathcal{T}(\hat{A}(\mathbf{x},-i\tau)\hat{B}(0)) \rangle \; , \tag{1.10}$$

using analytic continuation. This is easily seen from the spectral representation. The correlation function $G^E_{AB}(\mathbf{x},\tau)$ is a periodic function of imaginary-time (with period $\beta$); hence, its Fourier transform depends on a discrete frequency, $\nu_l = 2\pi l/\beta$, where $l$ is an integer, and has the spectral representation

$$\tilde{G}^E_{AB}(\mathbf{k}, i\nu_l) \equiv \int_0^\beta d\tau \int d^3\mathbf{x}\, e^{-i\mathbf{k}\cdot\mathbf{x}+i\nu_l\tau} \times \langle \mathcal{T}(\hat{A}(\mathbf{x},-i\tau)\hat{B}(0)) \rangle = \int \frac{d\omega}{2\pi} \, \frac{\rho_{AB}(\mathbf{k},\omega)}{\omega - i\nu_l} \; . \tag{1.11}$$

Comparing with the spectral representation (1.5) shows that the advanced function is given by the analytic continuation $\tilde{G}^E_{AB}(\mathbf{k},\omega+i\epsilon)$ and the retarded function is $\tilde{G}^E_{AB}(\mathbf{k},\omega-i\epsilon)$. Hence, to obtain the spectral density, one must analytically continue the frequency dependence of $\tilde{G}^E_{AB}$ from the discrete set $\{i\nu_l\}$ to an arbitrary complex value [12], and take the discontinuity across the real axis:

$$i\rho_{AB}(\mathbf{k},\omega) = {\rm Disc}\, \tilde{G}^E_{AB}(\mathbf{k},\omega) \equiv \tilde{G}^E_{AB}(\mathbf{k},\omega+i\epsilon) - \tilde{G}^E_{AB}(\mathbf{k},\omega-i\epsilon) \; . \tag{1.12}$$

The perturbative evaluation of finite temperature, imaginary-time correlation functions involves precisely the same momentum space diagrammatic rules as at zero temperature except for the replacement of frequency integrals by sums [1,13,14], $\int dk^0/2\pi \to (1/\beta)\sum_{\nu_l}$. In contrast with the matrix structure of the real-time propagator (1.6), the free scalar propagator for the perturbative calculation of imaginary-time correlation functions

is simply the usual

$$\tilde{G}_0^E(\mathbf{k}, i\nu_l) = \frac{1}{\nu_l^2 + \mathbf{k}^2 + m^2} \,. \tag{1.13}$$

For determining the spectral density, the drawback of the imaginary-time approach is that one must first manage to perform explicitly all the frequency summations. Only then can one analytically continue the external frequency and compute the discontinuity (1.12).

As shown in the next section, all the necessary frequency summations can be evaluated directly. Furthermore, one may perform these sums, analytically continue the external frequency, and take the discontinuity across the real axis before performing any of the remaining spatial momentum integrations. This process generates many terms from a single Feynman diagram, with individual terms corresponding to each possible "cutting" of an old-fashioned time-ordered diagram. These terms may be recombined to obtain simple expressions corresponding to "cut" Feynman diagrams which are generated by a set of rules that closely resemble the zero-temperature Cutkosky rules.

## II. FINITE TEMPERATURE PERTURBATION THEORY

Consider, for simplicity, a relativistic scalar field theory at nonzero temperature with vanishing chemical potential. By applying the standard momentum space Feynman rules, the perturbation series for a Fourier transformed imaginary-time correlation function may be generated. However, as the number of the loops increases, dealing with the discrete frequency summations becomes inconvenient. To avoid these frequency sums (at the cost of further integrals) one may simply Fourier transform (in time) the momentum space propagators. This yields "mixed" propagators that depend on a spatial momentum and imaginary time [15]. To evaluate this mixed propagator for a scalar theory, it is convenient to first write the momentum space propagator in terms of the free particle spectral density $\rho_0(\mathbf{k}, \omega)$:

$$\tilde{G}_0^E(\mathbf{k}, i\nu_l) = \frac{1}{\nu_l^2 + \mathbf{k}^2 + m^2} = \int \frac{d\omega}{2\pi} \frac{\rho_0(\mathbf{k}, \omega)}{\omega - i\nu_l} \,, \tag{2.1}$$

where

$$\rho_0(\mathbf{k}, \omega) = \frac{2\pi}{2E_k} \Big( \delta(\omega - E_k) - \delta(\omega + E_k) \Big) \,, \tag{2.2}$$

and $E_k = \sqrt{\mathbf{k}^2 + m^2}$. Then, using the relations

$$\frac{1}{\beta} \sum_{l=-\infty}^{\infty} e^{-i\nu_l \tau} \frac{1}{\omega - i\nu_l} = \theta(\tau) \frac{e^{-\omega\tau}}{1 - e^{-\beta\omega}} + \theta(-\tau) \frac{e^{-\omega\tau}}{e^{\beta\omega} - 1} \tag{2.3}$$

(valid in the interval $-\beta \le \tau \le \beta$), and $-n(-\omega) = [1 + n(\omega)]$, one obtains

$$\begin{aligned} \tilde{G}_0^E(\mathbf{k}, \tau) &= \sum_{l=-\infty}^{\infty} \tilde{G}_0^E(\mathbf{k}, i\nu_l)\, e^{-i\nu_l \tau} \\ &= \int_{-\infty}^{\infty} \frac{d\omega}{2\pi} \rho_0(\mathbf{k}, \omega)\, e^{-\omega\tau} \Big( \theta(\tau)[1 + n(\omega)] + \theta(-\tau) n(\omega) \Big) \\ &= \int_{-\infty}^{\infty} \frac{d\omega}{2\pi} \Big( 1 + n(\omega) \Big) \Big( \rho_0(\mathbf{k}, \omega)\, \theta(\tau) - \rho_0(\mathbf{k}, -\omega)\, \theta(-\tau) \Big) e^{-\omega|\tau|} \,. \end{aligned} \tag{2.4}$$

For the scalar field propagator, the rotational invariance of the system implies that the spectral density depends only on the magnitude of the momentum. Since the free spectral density (2.2) is an odd function of the frequency, the propagator takes the convenient form

$$\tilde{G}_0^E(|\mathbf{k}|, \tau) = \int_{-\infty}^{\infty} \frac{d\omega}{2\pi} \Big( 1 + n(\omega) \Big) \rho_0(|\mathbf{k}|, \omega)\, e^{-\omega|\tau|} \,. \tag{2.5}$$

This result may, of course, be derived directly using the free equation of motion plus periodicity in imaginary time.

As discussed in Appendix A, in the absence of a chemical potential, *CPT* invariance guarantees that the spectral density for the interacting scalar field propagator remains an odd function of the frequency. In what follows, this symmetry of the spectral density will play a role in simplifying the diagrammatic rules. We work with

$$-\mathcal{L} = \frac{1}{2}\phi(-\partial_\tau^2 - \nabla^2 + m^2)\phi + \frac{1}{4!}\lambda\phi^4 \,. \tag{2.6}$$

To evaluate a Feynman diagram for a two-point function using these "mixed" propagators, one labels each line by a spatial momentum and each vertex by a Euclidean time $\tau_j$ which will be integrated over from 0 to $\beta$. At each vertex where an external operator inserts external frequency $i\nu_j$, an additional factor of $\exp(i\nu_j\tau_j)$ is present. Each interaction vertex contributes a factor of $(-\lambda)$. Each line connecting two vertices labeled by the times $\tau_a$ and $\tau_b$ represents a propagator $\tilde{G}_0^E(|\mathbf{k}|, \tau_a - \tau_b)$. As usual, spatial momenta are conserved at every vertex, and all remaining spatial loop momenta are integrated over. Thus, the contribution of a diagram with a total of $n+1$ vertices and two operator insertions has the schematic form

$$C_{AB}^{(\Gamma)}(\mathbf{q},i\nu) \equiv \frac{(-\lambda)^{n-1}}{\mathcal{S}_\Gamma}\int_0^\beta d\tau_0\cdots d\tau_n \int \prod_{L\in\Gamma}\frac{d^3\mathbf{k}_L}{(2\pi)^3}\,\exp\Big\{i\nu\tau_l + i\nu'\tau_0\Big\} f_{AB}(\{\mathbf{k}_L\},\mathbf{q}) \times \prod_{\alpha\in\Gamma}\int\frac{dk_\alpha^0}{2\pi}\Big(1+n(k_\alpha^0)\Big)\,\rho_0(|\mathbf{k}_\alpha|,k_\alpha^0)\,\exp\Big\{-k_\alpha^0|\tau_a-\tau_b|\Big\}\,. \tag{2.7}$$

Here $\Gamma$ denotes the Feynman diagram under consideration, $\alpha$ labels the different lines of the graph, $\{\mathbf{k}_L\}$ are loop momenta, and $\mathcal{S}_\Gamma$ is the overall symmetry factor. The factor

$$f_{AB}(\{\mathbf{k}_L\},\mathbf{q}) \equiv f_A(\{\mathbf{k}_L\},\mathbf{q})\,f_B(\{\mathbf{k}_L\},\mathbf{q}) \tag{2.8}$$

represents the action of the external operators $\hat{A}$ and $\hat{B}$. It is only a function of spatial momenta provided that the operators do not contain any time derivatives of the elementary field. If they do contain time derivatives, then so does $f_{AB}(\{\mathbf{k}_L\},\mathbf{q})$. For simplicity, we will assume that no such time derivatives are present. The generalization to include operators with time derivatives is discussed in Appendix B; this presents minor complications but introduces no new features. The times $\tau_l$ and $\tau_0$ label the vertices where the external operators insert the external frequencies $i\nu$ and $i\nu'$ and $\{\tau_a,\tau_b\}$ are times within the set $\{\tau_0,\ldots,\tau_n\}$.

Because of the translational invariance in imaginary time, one can immediately do one time integration which generates an overall Kronecker delta function enforcing the conservation of the total external frequency, $i\nu+i\nu' = 0$. Equivalently, one may simply set $\tau_0$ to zero and assign $i\nu' = -i\nu$ to that vertex. Then, the remaining time integrals in $C_{AB}^{(\Gamma)}$ have the form

$$\mathcal{J} = \int_0^\beta d\tau_1\cdots d\tau_n\,\exp\Big\{i\nu\tau_l - \sum_\alpha k_\alpha^0|\tau_a-\tau_b|\Big\}\,, \tag{2.9}$$

with $\tau_0 \equiv 0$. The evaluation of this integral and the association of the result with old-fashioned time-ordered diagrams are the main subjects of this section. Performing these intermediate time integrations in this "mixed" form of perturbation theory is exactly equivalent to carrying out all the intermediate frequency summations in the Fourier transformed version of perturbation theory. After performing these integrations, it will be easy to analytically continue the external frequency in the resulting expression.

Before proceeding with the general analysis, it may be helpful to consider a simple example. The lowest-order connected term in the perturbative expansion of $\langle\mathcal{T}(\hat{\phi}^2(\mathbf{x},-i\tau)\hat{\phi}^2(0))\rangle$ is given by twice the square of the free propagator, $(G_0^E(\mathbf{x},\tau))^2$. The Fourier transform is

$$\begin{aligned}
\tilde{G}^{1\text{ loop}}_{\phi^2\phi^2}(\mathbf{q},i\nu) &\equiv 2\int d^3\mathbf{x}\int_0^\beta d\tau\, e^{-i\mathbf{q}\cdot\mathbf{x}+i\nu\tau}\Big(G_0^E(\mathbf{x},\tau)\Big)^2 \\
&= 2\int\frac{d^3\mathbf{k}}{(2\pi)^3}\int_0^\beta d\tau\, e^{i\nu\tau}\,\tilde{G}_0^E(|\mathbf{k}|,\tau)\,\tilde{G}_0^E(|\mathbf{q}-\mathbf{k}|,\tau) \\
&= 2\int\frac{d^3\mathbf{k}}{(2\pi)^3}\int_0^\beta d\tau\, e^{i\nu\tau}\int\frac{dk^0}{2\pi}\,e^{-k^0|\tau|}\Big(1+n(k^0)\Big)\,\rho_0(|\mathbf{k}|,k^0) \\
&\qquad\times\int\frac{dk'^0}{2\pi}\,e^{-k'^0|\tau|}\Big(1+n(k'^0)\Big)\,\rho_0(|\mathbf{q}-\mathbf{k}|,k'^0) \\
&= 2\int\frac{d^3\mathbf{k}}{(2\pi)^3}\int\frac{dk^0}{2\pi}\frac{dk'^0}{2\pi}\Big(1+n(k^0)\Big)\,\rho_0(|\mathbf{k}|,k^0)\Big(1+n(k'^0)\Big)\,\rho_0(|\mathbf{q}-\mathbf{k}|,k'^0)\,\frac{1-e^{-\beta(k^0+k'^0)}}{k^0+k'^0-i\nu}\,.
\end{aligned} \tag{2.10}$$

To simplify this, we may use $e^{-\beta k^0}\,[1+n(k^0)] = -[1+n(-k^0)]$, plus the fact that the spectral density of the propagator is an odd function of the frequency, to rewrite the result as

$$\tilde{G}^{1\text{ loop}}_{\phi^2\phi^2}(\mathbf{q},i\nu) = 2\int\frac{d^3\mathbf{k}}{(2\pi)^3}\int\frac{dk^0}{2\pi}\frac{dk'^0}{2\pi}\Big(1+n(k^0)\Big)\,\rho_0(|\mathbf{k}|,k^0)\Big(1+n(k'^0)\Big)\,\rho_0(|\mathbf{q}-\mathbf{k}|,k'^0) \times\left(\frac{1}{k^0+k'^0-i\nu}+\frac{1}{k^0+k'^0+i\nu}\right)\,. \tag{2.11}$$

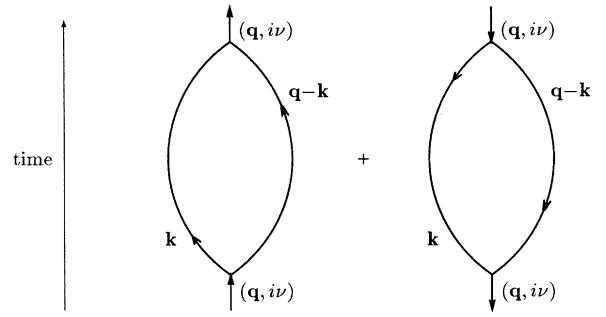


FIG. 1. The lowest order diagrams for the correlation function $\langle \mathcal{T}(\hat{\phi}^2(\mathbf{x}, i\tau)\hat{\phi}^2(0))\rangle$.

Aside from the fact that the external frequency is discrete and imaginary, the terms in the parentheses of Eq. (2.11) may be recognized as the standard energy denominators of time-dependent perturbation theory [16]. The integration over the spatial momentum $\mathbf{k}$ can be regarded as the sum over all intermediate two-particle states. Thus it is natural to associate the two terms in Eq. (2.11) with old-fashioned time-ordered perturbation theory diagrams as illustrated in Fig. 1. The time ordering of the first diagram corresponds to the energy denominator $(k^0+k'^0-i\nu)$, and the time ordering of the second diagram corresponds to the energy denominator $(k^0+k'^0+i\nu)$. In both cases, the energy denominator can be interpreted as the sum of frequencies of lines crossing the interval between two external vertices minus the external frequency flowing out of the vertex above the interval. The contribution of a line with momentum $(\mathbf{k}, k^0)$ is given by $[1+n(k^0)]\,\rho_0(|\mathbf{k}|, k^0)$, which, in the zero temperature limit, reduces to $\theta(k^0)2\pi\delta(k^2+m^2)$. The integration over the spatial loop momentum and frequencies $k^0$ and $k'^0$ completes the expression.

This association of the result of the imaginary-time integrations (or equivalently the discrete frequency summation) with old-fashioned time-ordered diagrams is a general result. To see this, we now go back to the evaluation of the time integral in (2.9):

$$\mathcal{J} = \int_0^\beta d\tau_1 \cdots d\tau_n \, \exp\left\{ i\nu\tau_l \, - \sum_\alpha k_\alpha^0 |\tau_a - \tau_b| \right\} ,$$

and split the integrand into $n!$ terms according to the relative orderings of the $n$ different time variables. The term corresponding to a particular time ordering, for example, $\tau_n \geq \tau_{n-1} \geq \cdots \geq \tau_2 \geq \tau_1$, may be written as

$$\mathcal{I}(\{k_\alpha^0\}, i\nu) \equiv \int_0^\beta d\tau_n \cdots \int_0^{\tau_3} d\tau_2 \int_0^{\tau_2} d\tau_1 \, \exp\left\{ \sum_{s=1}^n -\sigma_s \tau_s \right\} , \tag{2.12}$$

where

$$\sigma_s \equiv \omega_{\rm in}^s - \omega_{\rm out}^s - i\nu_s \, , \tag{2.13}$$

with

$$\omega_{\rm in}^s \equiv \sum_{\substack{\alpha \in \{(s) \leftrightarrow \\ (0,1,2,\ldots,s-1)\}}} k_\alpha^0 \, , \tag{2.14}$$

and

$$\omega_{\rm out}^s \equiv \sum_{\substack{\alpha \in \{(s) \leftrightarrow \\ (s+1,s+2,\ldots,n)\}}} k_\alpha^0 \, . \tag{2.15}$$

Here $\{(a, \ldots, b) \leftrightarrow (c, \ldots, d)\}$ indicates the set of lines connecting vertices at times $\{\tau_a, \ldots, \tau_b\}$ with those at times $\{\tau_c, \ldots, \tau_d\}$. Hence $\omega_{\rm in}^s$ is the sum of frequencies of all lines connecting $\tau_s$ with earlier times $\{\tau_0, \tau_1, \tau_2, \ldots, \tau_{s-1}\}$, and $\omega_{\rm out}^s$ is the sum of frequencies of the lines connecting $\tau_s$ with later times $\{\tau_{s+1}, \tau_{s+2}, \ldots, \tau_n\}$. The discrete external frequency $i\nu_s$ is given by $i\nu\,\delta_{sl}$ because the external frequency is inserted only at the vertex labeled by $\tau_l$. The contributions of all the other time orderings may be brought to this same form by suitably renaming the time variables.

To facilitate the evaluation of the time integral $\mathcal{I}(\{k_\alpha^0\}, i\nu)$, consider the sequence of integrals

$$\mathcal{I}_n(\tau) \equiv \int_0^\tau d\tau_n \, e^{-\sigma_n \tau_n} \int_0^{\tau_n} d\tau_{n-1} \, e^{-\sigma_{n-1}\tau_{n-1}} \cdots \times \int_0^{\tau_2} d\tau_1 \, e^{-\sigma_1 \tau_1} \, , \tag{2.16}$$

with the initial condition $\mathcal{I}_0(\tau) \equiv 1$. The original time integral is $\mathcal{I}(\{k_\alpha^0\}, i\nu) = \mathcal{I}_n(\beta)$. The functions $\mathcal{I}_n(\tau)$ satisfy

$$\frac{d}{d\tau}\mathcal{I}_n(\tau) = e^{-\sigma_n \tau}\mathcal{I}_{n-1}(\tau) \, . \tag{2.17}$$

This differential relation implies a simple algebraic recursion relation for the Laplace transforms of the $\mathcal{I}_n(\tau)$:

$$\begin{aligned} \mathcal{L}_n(\lambda) &\equiv \int_0^\infty d\tau \, e^{-\lambda\tau} \mathcal{I}_n(\tau) \\ &= \int_0^\infty d\tau \left( \frac{-1}{\lambda} \frac{d}{d\tau} e^{-\lambda\tau} \right) \mathcal{I}_n(\tau) \\ &= \frac{1}{\lambda} \int_0^\infty d\tau \, e^{-\lambda\tau} \frac{d}{d\tau} \mathcal{I}_n(\tau) \\ &= \frac{1}{\lambda} \int_0^\infty d\tau \, e^{-\lambda\tau - \sigma_n \tau} \, \mathcal{I}_{n-1}(\tau) \\ &= \frac{1}{\lambda} \mathcal{L}_{n-1}(\lambda + \sigma_n) \, . \end{aligned} \tag{2.18}$$

Iterating this equation produces

$$\begin{aligned} \mathcal{L}_n(\lambda) &= \frac{1}{\lambda} \frac{1}{\lambda+\sigma_n} \frac{1}{\lambda+\sigma_n+\sigma_{n-1}} \cdots \frac{1}{\lambda+\sigma_n+\cdots+\sigma_1} \\ &= \frac{1}{\lambda} \prod_{j=1}^n \frac{1}{\lambda+\Omega_j^n} \, , \end{aligned} \tag{2.19}$$

where we have defined

$$\Omega_j^n \equiv \sum_{s=j}^{n} \sigma_s \,. \tag{2.20}$$

The original integral is recovered by performing an inverse Laplace transform:

$$\mathcal{I}_n(\tau) = \int_{\gamma-i\infty}^{\gamma+i\infty} \frac{d\lambda}{2\pi i}\, e^{\lambda\tau}\, \mathcal{L}_n(\lambda) \,, \tag{2.21}$$

where $\gamma > \Omega_j^n$ for all $j \le n$. Closing the contour anticlockwise at infinity and picking up the residues of all the poles yields

$$\begin{aligned}
\mathcal{I}_n(\beta) &= \mathcal{I}(\{k_\alpha^0\}, i\nu) \\
&= \prod_{j=1}^{n} \frac{1}{\Omega_j^n} + \sum_{k=1}^{n} e^{-\beta\Omega_k^n} \frac{1}{-\Omega_k^n} \prod_{\substack{j=1 \\ j\neq k}}^{n} \frac{1}{\Omega_j^n - \Omega_k^n} \\
&= \prod_{j=1}^{n} \frac{1}{\Omega_j^n} + \sum_{k=1}^{n} e^{-\beta\Omega_k^n} \prod_{j=1}^{k-1} \frac{1}{\Omega_j^{k-1}} \prod_{j'=k+1}^{n+1} \frac{1}{-\Omega_k^{j'-1}} \\
&= \sum_{k=1}^{n+1} e^{-\beta\Omega_k^n} \prod_{j=1}^{k-1} \frac{1}{\Omega_j^{k-1}} \prod_{j'=k+1}^{n+1} \frac{1}{-\Omega_k^{j'-1}} \\
&= \sum_{k=0}^{n} e^{-\beta\Omega_{k+1}^n} \left( \prod_{j=1}^{k} \Omega_j^k \prod_{j'=k+1}^{n} (-\Omega_{k+1}^{j'}) \right)^{-1} ,
\end{aligned} \tag{2.22}$$

where

$$\Omega_j^k \equiv \Omega_j^n - \Omega_{k+1}^n \tag{2.23}$$

and in the last two lines a product that has no elements is to be interpreted as 1 and $e^{-\beta\Omega_{n+1}^n} \equiv 1$.

The time integral $\mathcal{I}(\{k_\alpha^0\}, i\nu)$ (2.12) is an analytic function of the real frequencies; i.e., all derivatives exist and are finite. Thus, although individual terms in the expression (2.22) may become singular when any of the factors in the denominator vanishes, the whole expression must give the correct value of the finite integral if the limiting value is taken as the value of the expression (2.22). Since the function $\mathcal{I}$ is analytic, how one approaches the limiting point is irrelevant. For our purpose, it will be convenient to approach the limiting points from just off the real lines in the complex space of frequencies $\{k_\alpha^0\}$. Equivalently, it will be convenient to regulate the expression (2.22) by adding an infinitesimal imaginary part $i\epsilon_s$ to each frequency sum $\sigma_s$ so that none of the denominator factors vanish for any real value of momenta and the frequencies. Any set of infinitesimal imaginary parts may be used as long as these conditions are met. Different choices produce equivalent results for $\mathcal{I}$, but create differing pole structure in individual terms. Since the rules derived in this section involve each individual term, a different choice of infinitesimal imaginary parts can lead to a different set of rules. The most convenient choice is the one which leads to the standard Cutkosky rules in the zero temperature limit. The following choice of the infinitesimal parts does this. Define

$$\mathcal{I}(\{k_\alpha^0\}, i\nu) = \lim_{\epsilon\to 0} \sum_{k=0}^{n} \left( \prod_{j=1}^{k} (\Omega_j^k - i\epsilon_j^k) \prod_{j'=k+1}^{n} (-\Omega_{k+1}^{j'} + i\epsilon_{k+1}^{j'}) \right)^{-1} \exp\left\{\beta(-\Omega_{k+1}^n + i\epsilon_{k+1}^n)\right\} \,, \tag{2.24}$$

where

$$\epsilon_p^n \equiv \begin{cases} (n-p+1)\epsilon & \text{for } l+1 \le p \le n, \\ (n+p-l)\epsilon & \text{for } 1 \le p \le l, \end{cases} \tag{2.25}$$

and

$$\epsilon_j^k \equiv \epsilon_j^n - \epsilon_{k+1}^n \,. \tag{2.26}$$

Here the index $l$ corresponds to the vertex at time $\tau_l$ where the external frequency is inserted.

For further simplification of Eq. (2.24), we need to examine the structure of the factors in $\mathcal{I}$ more closely. In view of the definition Eq. (2.13), the factor $\Omega_j^k = \sum_{s=j}^{k} \sigma_s$ contains the sum of frequencies of all the lines connected to any of the times $\{\tau_j, \tau_{j+1}, \ldots, \tau_k\}$ with signs indicating whether the line comes from an earlier time $(+\omega_{\text{in}}^s)$ or a later time $(-\omega_{\text{out}}^s)$. Among these frequencies, those corresponding to the lines connecting the times $\{\tau_j, \tau_{j+1}, \ldots, \tau_k\}$ to themselves cancel in the sum for $\Omega_j^k$. Hence

$$\operatorname{Re}\Omega_j^k = \sum_{\alpha\in\Lambda_{\text{in}}^{j,k}} k_\alpha^0 - \sum_{\alpha'\in\Lambda_{\text{out}}^{j,k}} k_{\alpha'}^0 \,, \tag{2.27}$$

where, as illustrated in Fig. 2, $\Lambda_{\text{in}}^{j,k}$ indicates the set of lines connecting the times $\{\tau_j, \tau_{j+1}, \ldots, \tau_k\}$ with the earlier times $\{\tau_0, \tau_1, \tau_2, \ldots, \tau_{j-1}\}$, and $\Lambda_{\text{out}}^{j,k}$ indicates a set of lines connecting the times $\{\tau_j, \tau_{j+1}, \ldots, \tau_k\}$ with the later times $\{\tau_{k+1}, \tau_{k+2}, \ldots, \tau_n\}$. In particular,

$$\operatorname{Re}\Omega_k^n = \sum_{\alpha\in\Lambda_{\text{in}}^{k,n}} k_\alpha^0 \,, \tag{2.28}$$

so that the exponential in Eq. (2.24) has the form

$$\exp\Big\{\beta(-\Omega_k^n + i\epsilon_k^n)\Big\} = \exp\Big\{i\beta\epsilon_k^n - \sum_{\alpha\in\Lambda_{\text{in}}^{k,n}} \beta k_\alpha^0\Big\} \,. \tag{2.29}$$

In the expression (2.7) for the result of the complete graph, the time integral $\mathcal{I}$ is multiplied by frequency integrals containing Bose-Einstein factors and the spectral densities of free propagators. Since the Bose-Einstein factors satisfy $e^{-\beta\omega}\,[1+n(\omega)] = n(\omega)$, and the spectral densities are odd functions of the frequency, the identity

$$\int \frac{d\omega}{2\pi}\Big(1+n(\omega)\Big)\,\rho_0(\omega)\,e^{-\beta\omega}\,f(\omega)$$

$$= \int \frac{d\omega}{2\pi}\,n(\omega)\,\rho_0(\omega)\,f(\omega)$$

$$= \int \frac{d\omega}{2\pi}\Big(1+n(\omega)\Big)\,\rho_0(\omega)\,f(-\omega) \quad (2.30)$$

holds for any function $f(\omega)$. This identity may be used to absorb the factors of $e^{-\beta \mathrm{Re}\,\Omega^n_{k+1}}$ appearing in the result (2.24) for the time integral $\mathcal{I}$. When inserted into the expression for the complete graph, the factor of $e^{-\beta \mathrm{Re}\,\Omega^n_{k+1}}$ in each term of $\mathcal{I}$ may be omitted if, at the same time, the sign of all frequencies in the set $\Lambda_{\rm in}^{k+1,n}$ are changed in the corresponding denominator.[3]

To see the effect of this sign change on the remaining factors of $\Omega^k_j$ in the denominator, recall that $\mathrm{Re}\,\Omega^k_j$ is the sum of the incoming frequencies of the lines $\Lambda_{\rm in}^{j,k}$ entering the block of the times $\{\tau_k,\ldots,\tau_j\}$ minus the sum of outgoing frequencies of the lines $\Lambda_{\rm out}^{j,k}$ leaving the block. To be a member of the set $\Lambda_{\rm out}^{j,k}$, a line must cross the interval just above the latest time in the time block, $\tau_k$. All lines that cross this interval are also members of $\Lambda_{\rm in}^{k+1,n}$ since $\Lambda_{\rm in}^{k+1,n}$ consists of all lines that cross the same interval. Thus when the exponential factor $e^{-\beta \mathrm{Re}\,\Omega^n_{k+1}}$ is absorbed, all outgoing frequencies in $\mathrm{Re}\,\Omega^k_j$ change sign. On the other hand, none of the lines corresponding to the incoming frequencies for the set of times $\{\tau_k,\ldots,\tau_j\}$ are members of $\Lambda_{\rm in}^{k+1,n}$ because these incoming lines all terminate at times earlier than $\tau_{k+1}$. Thus the incoming frequencies are not affected by the absorption of the exponential factor. Hence, after this change of variables, $\mathrm{Re}\,\Omega^k_j$ is replaced by the frequency sum

$$\Lambda^k_j \equiv \sum_{\alpha\in\Lambda_{\rm in}^{j,k}} k^0_\alpha + \sum_{\alpha'\in\Lambda_{\rm out}^{j,k}} k^0_{\alpha'}\,. \quad (2.31)$$

Note that $\Lambda^k_j$ is the sum of frequencies of all lines that connect any of the times $\{\tau_k,\ \tau_{k-1},\ldots,\ \tau_j\}$ to times outside of this set. A similar result holds for the factors involving $\mathrm{Re}\,\Omega^{j'}_{k+1}$. In this case, it is the incoming frequencies that change sign and $\mathrm{Re}\,\Omega^{j'}_{k+1}$ is replaced by

$$-\Lambda^{j'}_{k+1} \equiv -\sum_{\alpha\in\Lambda_{\rm in}^{k+1,j'}} k^0_\alpha - \sum_{\alpha'\in\Lambda_{\rm out}^{k+1,j'}} k^0_{\alpha'}\,, \quad (2.32)$$

which is minus the sum of frequencies of all lines that connect any of the times $\{\tau_{j'},\ \tau_{j'-1},\ldots,\ \tau_{k+1}\}$ to times outside of this set.

Consequently, the expression (2.24) for the result of the time integration may be replaced by the equivalent result

$$\mathcal{I}(\{k^0_\alpha\},i\nu) = \sum_{k=0}^{n} S_k(\{k^0_\alpha\},i\nu)\,e^{i\beta\epsilon^n_{k+1}}\,, \quad (2.33)$$

where, for $n\ge k\ge l$,

$$S_k(\{k^0_\alpha\},i\nu) \equiv \prod_{j=1}^{l}\Big(\Lambda^k_j - i\nu - i\epsilon^k_j\Big)^{-1} \prod_{j'=l+1}^{k}\Big(\Lambda^k_{j'} - i\epsilon^k_{j'}\Big)^{-1} \prod_{j''=k+1}^{n}\Big(\Lambda^{j''}_{k+1} + i\epsilon^{j''}_{k+1}\Big)^{-1}\,, \quad (2.34a)$$

and

$$S_k(\{k^0_\alpha\},i\nu) \equiv \prod_{j=1}^{k}\Big(\Lambda^k_j - i\epsilon^k_j\Big)^{-1} \prod_{j'=k+1}^{l-1}\Big(\Lambda^{j'}_{k+1} + i\epsilon^{j'}_{k+1}\Big)^{-1} \prod_{j''=l}^{n}\Big(\Lambda^{j''}_{k+1} + i\nu + i\epsilon^{j''}_{k+1}\Big)^{-1}\,, \quad (2.34b)$$

for $l-1\ge k\ge 0$.

The exponential factor $e^{i\beta\epsilon^n_{k+1}}$ in Eq. (2.33) cannot be omitted if two or more lines share the same energy. In that case, the spectral densities of the propagators may cause some of the factors in the denominator of $S_k$ to vanish (except for the $i\epsilon$'s) for all values of the spatial loop momenta. Then terms of order $\epsilon$ and higher in the expansion of the exponential can result in finite contributions and hence must be kept. For the purpose of deriving simple diagrammatic rules, this is an inconvenience. To avoid this, note that if the external four-momentum is nonzero, only self-energy insertions can cause multiple lines to have identical four-momentum. If all self-energy

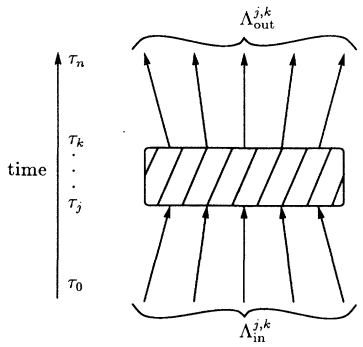


FIG. 2. Illustration of the sets of lines $\Lambda^{j,k}_{\rm in}$ and $\Lambda^{j,k}_{\rm out}$. The shaded box contains the vertices labeled with $\{\tau_j,\cdots,\tau_k\}$ and the lines connected to themselves. The set $\Lambda^{j,k}_{\rm in}$ contains the lines going into the box while $\Lambda^{j,k}_{\rm out}$ contains those coming out of the box.

[3]If the external operators involve time derivatives, the corresponding factors in the numerator must also be changed.

insertions are resummed, thereby replacing bare propagators by fully dressed one-particle propagators, then no self-energy insertions remain and the factor $e^{i\beta\epsilon_{k+1}^n}$ may be set to one. The full propagator is given by

$$\tilde{G}^E(|\mathbf{k}|, i\nu) \equiv \frac{1}{\nu^2 + E_k^2 + \Sigma(|\mathbf{k}|, i\nu)} , \tag{2.35}$$

where $\Sigma(|\mathbf{k}|, i\nu)$ is the full one-particle self-energy in the imaginary-time formulation. The spectral density of this propagator is given by

$$\begin{aligned} i\rho(|\mathbf{k}|, \omega) &\equiv \tilde{G}^E(|\mathbf{k}|, \omega{+}i\epsilon) - \tilde{G}^E(|\mathbf{k}|, \omega{-}i\epsilon) \\ &= \left[E_k^2 - (\omega{+}i\epsilon)^2 + \Sigma(|\mathbf{k}|, \omega{+}i\epsilon)\right]^{-1} \\ &\quad - \left[E_k^2 - (\omega{-}i\epsilon)^2 + \Sigma(|\mathbf{k}|, \omega{-}i\epsilon)\right]^{-1} , \end{aligned} \tag{2.36}$$

and the corresponding "mixed" propagator is

$$\tilde{G}^E(|\mathbf{k}|, |\tau|) = \int \frac{d\omega}{2\pi} \Big(1 + n(\omega)\Big)\, \rho(|\mathbf{k}|, \omega)\, e^{-\omega|\tau|} . \tag{2.37}$$

Note that the calculation of the spectral density also requires the analytic continuation of the self-energy.

From now on, unless stated explicitly otherwise, the fully dressed one-particle propagator will be used and the term "skeleton expansion" will denote the expansion in which the propagators are fully dressed but the vertices are not. Of course, for a practical calculation, some approximation of the full propagator must be made. Because of infrared divergences, performing a consistent expansion in the powers of the coupling constant may not be completely trivial [14]. This will be discussed further in Sec. V.

We return now to the original time integral (2.9). Recall that the integral $\mathcal{I}$ was one of the $n!$ different time orderings in the complete integral $\mathcal{J}$. As shown in Eq. (2.33), each different time ordering generates a sum of $n{+}1$ individual terms. Hence, there are a total of $(n{+}1)!$ terms contributing to $\mathcal{J}$. These correspond precisely to the $(n{+}1)!$ different time orderings of the $n{+}1$ vertices in the original graph (including the one vertex whose time was set to zero). In particular, each term in the result (2.33) is naturally associated with a cyclic permutation of the $n{+}1$ times, $\tau_n \geq \cdots \geq \tau_1 \geq 0$. This may be seen as follows. Consider the real part of the factors $\Lambda_j^k$ and $\Lambda_{k+1}^{j''}$ appearing in the denominator of $S_k$. As noted earlier, $\Lambda_j^k$ is the sum of frequencies of all lines that connect any of the times $\{\tau_k, \tau_{k-1}, \ldots, \tau_j\}$ to times outside of this set. Equivalently, when the time ordering starts with the sequence $\tau_k \geq \tau_{k-1} \geq \cdots \geq \tau_j \geq \cdots$, $\Lambda_j^k$ is the sum of frequencies of all lines crossing the interval preceding $\tau_j$, since for this ordering, any line connected to any of the times $\{\tau_k, \tau_{k-1}, \ldots, \tau_j\}$ from outside this set must cross the interval just below the earliest time in the set, $\tau_j$. Similarly, $\Lambda_{k+1}^{j''}$ is the sum of frequencies of all lines that connect any of the times $\{\tau_{j''}, \ldots, \tau_{k+2}, \tau_{k+1}\}$ to times outside of this set. Equivalently, it can be interpreted as the sum of frequencies of all lines crossing the interval just above $\tau_{j''}$ when the time ordering ends with $\cdots \geq \tau_{j''} \geq \cdots \geq \tau_{k+2} \geq \tau_{k+1}$. In this case, a line connected to any of the times $\{\tau_{j''}, \ldots, \tau_{k+2}, \tau_{k+1}\}$ from outside this set must cross the interval just above the largest time in the set, $\tau_{j''}$.

Since $j$ ranges from 1 to $k$ and $j''$ ranges from $k{+}1$ to $n$, these completely determine the time ordering, $\tau_k \geq \tau_{k-1} \geq \cdots \geq \tau_1 \geq 0 \geq \tau_n \geq \tau_{n-1} \geq \cdots \geq \tau_{k+1}$. Hence, each denominator factor of $\Lambda_j^k$ and $\Lambda_{k+1}^{j''}$ can be interpreted as the sum of frequencies of all lines crossing each interval in this time ordering. The external frequency contributions have a similar interpretation. When $\tau_l > \tau_0$, the frequency denominators of $S_k$ corresponding to intervals between $\tau_l$ and $\tau_0 \equiv 0$ contain $-i\nu$. Since external frequency $i\nu$ flows out of the vertex labeled with $\tau_l$ and flows into the vertex labeled with $\tau_0$, the contribution $-i\nu$ is always minus the sum of external frequencies flowing out of the graph from above the interval. A similar interpretation is also possible when $\tau_0 > \tau_l$. In this case, the denominator factors of $S_k$ corresponding to the intervals between $\tau_0$ and $\tau_l$ contain $+i\nu$. Since the ordering of $\tau_l$ and $\tau_0$ is reversed compared to the previous case, again $+i\nu$ equals the sum of external frequencies flowing out of the vertices above the interval. Finally, this interpretation also holds for intervals which are not between the two external vertices. The part of the diagram above both $\tau_0$ and $\tau_l$ has no external vertex above it. Thus the net external frequency flow is zero; the part of the diagram below both $\tau_0$ and $\tau_l$ has two external vertices above it, and the net external frequency flow is again zero.

In this way, each contribution $S_k$ is associated with the cyclic permutation of the $n{+}1$ times, $\tau_n \geq \cdots \geq \tau_1 \geq 0$. Figure 3 schematically illustrates $S_n$. Figure 4 shows a term $S_k$ with $n > k \geq l$, while Fig. 5 shows $S_k$ with $l > k \geq 0$.

The assignment of infinitesimal $i\epsilon$'s in the denominator of the result (2.24) may seem complicated. But only the following two properties are necessary. First,

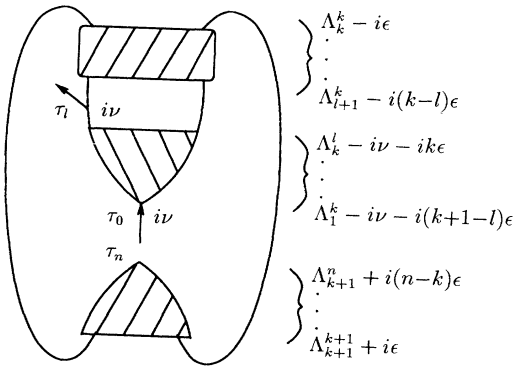


FIG. 4. A schematic illustration of $S_k$ with $n > k \geq l$. This diagram is cyclically related to the diagram in Fig. 3. The denominators from each interval are shown at the right. The upper shaded box contains times $\tau_{l+1}$ to $\tau_k$ and lines connected to them. The middle shaded box contains times $\tau_0$ to $\tau_{l-1}$ and lines connected to them. The lower shaded box contains times $\tau_{k+1}$ to $\tau_n$ and lines connected to them.

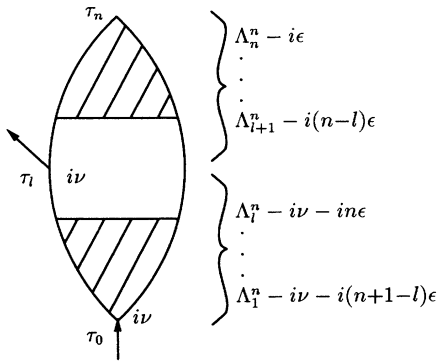


FIG. 3. A schematic illustration of $S_n$. The denominators from each interval is shown at the right. The upper shaded box contains times $\tau_{l+1}$ to $\tau_n$ and lines connecting them. The lower shaded box contains times $\tau_0$ to $\tau_{l-1}$ and lines connecting them. At the times $\tau_0$ and $\tau_l$, two external operators are inserted. The $\Lambda_s^n$ denotes the sum of all frequencies of the lines crossing the interval between $\tau_{s-1}$ and $\tau_s$.

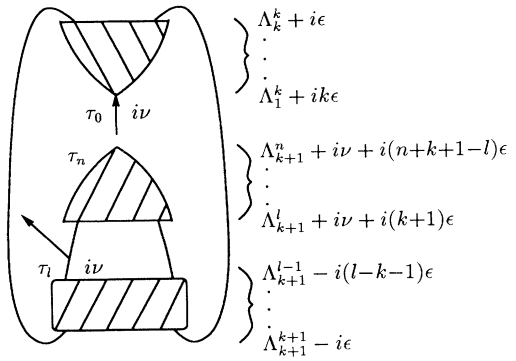


FIG. 5. A schematic illustration of $S_k$ with $l > k \geq 0$. This is also cyclically related to the diagram in Fig. 3. The denominators from each interval are shown explicitly at the right. The upper shaded box contains times $\tau_0$ to $\tau_k$ and lines connected to them. The middle shaded box contains times $\tau_{l+1}$ to $\tau_n$ and lines connected to them. The lower shaded box contains times $\tau_{k+1}$ to $\tau_{l-1}$ and lines connected to them.

the contributions of intervals above the vertex $\tau_l$ when $\tau_l > \tau_0$, as well as the contributions of intervals below $\tau_l$ when $\tau_0 > \tau_l$, all have negative imaginary infinitesimals, while contributions of intervals below the vertex $\tau_0$ when $\tau_l > \tau_0$, and the contributions of intervals above $\tau_0$ when $\tau_0 > \tau_l$, all have positive imaginary infinitesimals. Note that the contributions from these intervals do not contain the external frequency $i\nu$. Since the factors without $i\nu$ are not affected by taking the discontinuity across the real line in the complex $i\nu$ plane, only the signs of imaginary infinitesimals in the contributions from these intervals matter, but not their relative amplitudes. Second, between $\tau_l$ and $\tau_0$, starting from $\tau_l$, the infinitesimal imaginary part increases in each successive interval. These two conditions will be needed to simplify the final result and relate it to the standard Cutkosky rules.

In summary, in this section the following has been shown. When evaluating a Feynman diagram in the imaginary-time formulation, the intermediate frequency summations can be performed before any other calculation. Each term of the result may be naturally associated with an old-fashioned time-ordered perturbation theory diagram. The contribution of each time-ordered diagram is given by the product of frequency denominators from each time interval multiplied by a statistical factor and spectral density for each line. Hence a given Feynman diagram $\Gamma$ generates a contribution of the form[4]

$$C_{AB}^{(\Gamma)}(\mathbf{q}, i\nu) \equiv \frac{(-\lambda)^{n-1}}{\mathcal{S}_\Gamma} \int \prod_{L\in\Gamma} \frac{d^3\mathbf{k}_L}{(2\pi)^3} \prod_{\alpha\in\Gamma} \frac{dk_\alpha^0}{2\pi} \Big(1 + n(k_\alpha^0)\Big) \rho(|\mathbf{k}_\alpha|, k_\alpha^0) f_{AB}(\{\mathbf{k}_L\}, \mathbf{q}) \left( \sum_{\Gamma_\sigma\subset\Gamma} S_{\Gamma_\sigma}(\{k_\alpha^0\}, i\nu) \right) , \tag{2.38}$$

where $\Gamma_\sigma$ labels the different time-ordered diagrams and $S_{\Gamma_\sigma}$ is the product of frequency denominators:

$$S_{\Gamma_\sigma} \equiv \prod_{\substack{\text{intervals}\\ j}} \Big(\Lambda_j - i\nu_j - i\epsilon_j\Big)^{-1} . \tag{2.39}$$

Here $\Lambda_j$ is the sum of frequencies of all lines crossing the given interval, and $i\nu_j$ is the net external frequency flowing out of the diagram above the given interval. The vertices in a given time-ordered diagram can always be chronologically relabeled so that the largest time is $\tau_n$ and the smallest $\tau_0$. Then

$$\Lambda_j = \sum_{\alpha\in\Lambda_{\text{in}}^{j,n}} k_\alpha^0 \tag{2.40}$$

and

$$i\nu_j = i\nu\Big(\theta(l-j+1/2) - \theta(m-j+1/2)\Big) , \tag{2.41}$$

where $\tau_l$ labels the vertex where external frequency flows out (corresponding to the insertion of the operator $\hat{A}$) and $\tau_m$ labels the vertex where the external frequency flows in (corresponding to the insertion of the operator $\hat{B}$). As before, the subscript $\alpha$ labels the different lines, $L$ labels the different loops, and $\mathcal{S}_\Gamma$ denotes the overall symmetry factor associated with the diagram. The factor $f_{AB}(\{\mathbf{k}_L\}, \mathbf{q})$ represents the action of the external operators. Assigning the infinitesimal imaginary part $i\epsilon_j$ is a little complicated. For diagrams with $\tau_l > \tau_m$ (where operator $\hat{A}$ acts after $\hat{B}$),

[4]A similar result can be found in Ref. [23], which uses a different method to sum the intermediate frequencies.

$$\epsilon_j \equiv \begin{cases} \epsilon & \text{for } l{+}1 \le j \le n, \\ (j-m)\epsilon & \text{for } m{+}1 \le j \le l, \\ -\epsilon & \text{for } 1 \le j \le m, \end{cases} \tag{2.42}$$

while for diagrams with $\tau_m > \tau_l$ the assignments are reversed,

$$\epsilon_j \equiv \begin{cases} -\epsilon & \text{for } m{+}1 \le j \le n, \\ (m-j+1)\epsilon & \text{for } l{+}1 \le j \le m \\ \epsilon & \text{for } 1 \le j \le l \ . \end{cases} \tag{2.43}$$

Between $\tau_l$ and $\tau_m$, starting from $\tau_l$, the magnitude of $\epsilon_j$ decreases in each successive interval. For intervals before, or after, the action of both operators, only the sign of the imaginary part $\epsilon_j$ will matter.

## III. EVALUATING THE DISCONTINUITY

To find the spectral density, one must take the discontinuity of the analytically continued two-point function across the real axis in the complex frequency plane:

$$i\rho_{AB}(\mathbf{q},\omega) \equiv \tilde{G}^E_{AB}(\mathbf{q},\omega+i\epsilon) - \tilde{G}^E_{AB}(\mathbf{q},\omega-i\epsilon) \ . \tag{3.1}$$

Once the imaginary-time integrations are done, performing the analytic continuation in the external frequency is trivial. Furthermore, it is possible to take the discontinuity before any spatial loop momenta integral is evaluated.

The only source of a discontinuity comes from the product of energy denominators denoted by $S_{\Gamma_\sigma}$ in the previous result (2.38). To evaluate the discontinuity, it is convenient first to make a partial fraction expansion of $S_{\Gamma_\sigma}$. This simply means repeatedly using the identity

$$\frac{1}{XY} = \left(\frac{1}{Y} - \frac{1}{X}\right)\frac{1}{X-Y} \tag{3.2}$$

to write $S_{\Gamma_\sigma}$ as a sum of simple poles in the external frequency. The standard identity

$$\mathrm{Disc}\,\frac{1}{x} = \frac{1}{x+i\epsilon} - \frac{1}{x-i\epsilon} = -2\pi i\delta(x) \tag{3.3}$$

may then be applied. If the vertex $\tau_l$ where the external frequency flows out is above the vertex $\tau_m$ where the external frequency flows in, one obtains

$$\begin{aligned}\mathrm{Disc}\,S_{\Gamma_\sigma}(\{k^0_\alpha\},\omega) &\equiv S_{\Gamma_\sigma}(\{k^0_\alpha\},\omega+i\epsilon) - S_{\Gamma_\sigma}(\{k^0_\alpha\},\omega-i\epsilon) \\ &= \sum_{c=m+1}^{l}\prod_{j=l+1}^{n}\Big(\Lambda_j - i\epsilon\Big)^{-1}\prod_{p=c+1}^{l}\Big(\Lambda_p - \omega - i(\epsilon_p-\epsilon_c)\Big)^{-1} \\ &\quad\times(2\pi i)\delta(\Lambda_c-\omega)\prod_{q=m+1}^{c-1}\Big(\Lambda_q - \omega + i(\epsilon_c-\epsilon_q)\Big)^{-1}\prod_{j'=1}^{m}\Big(\Lambda_{j'}+i\epsilon\Big)^{-1}.\end{aligned} \tag{3.4a}$$

Alternatively, if the vertex $\tau_l$ where the external frequency flows out is below the vertex $\tau_m$ where the external frequency flows in, the discontinuity is given by

$$\begin{aligned}\mathrm{Disc}\,S_{\Gamma_\sigma}(\{k^0_\alpha\},\omega) &\equiv \sum_{c=l+1}^{m}\prod_{j=m+1}^{n}\Big(\Lambda_j + i\epsilon\Big)^{-1}\prod_{p=c+1}^{m}\Big(\Lambda_p + \omega + i(\epsilon_c-\epsilon_p)\Big)^{-1} \\ &\quad\times(-2\pi i)\delta(\Lambda_c+\omega)\prod_{q=l+1}^{c-1}\Big(\Lambda_q + \omega - i(\epsilon_q-\epsilon_c)\Big)^{-1}\prod_{j'=1}^{l}\Big(\Lambda_{j'}-i\epsilon\Big)^{-1}.\end{aligned} \tag{3.4b}$$

The sum (with index $c$) runs over the different poles in external frequency of $S_{\Gamma_\sigma}$, or equivalently, enumerates each interval between the two external vertices. Typical diagrams corresponding to these results are illustrated in Figs. 6 and 7. After taking the discontinuity, only the signs of the infinitesimal imaginary part matters; the relative magnitudes of $\epsilon_j$'s are no longer relevant. The combinations of $\epsilon_j$'s appearing in the above expression are all positive. Thus every infinitesimal in the above expression may be replaced by the same $i\epsilon$.

Each term of the discontinuity is naturally associated with a "cut" time-ordered diagram. This is a time-ordered diagram with a line, called the "cut," drawn across one time interval which must lie between the two external vertices. The result (3.4) is written in such a way that the contributions of the later intervals in a cut diagram appear earlier in the expression. The complete contribution of each cut diagram may obviously be factored to the product form:

$$\begin{aligned}\mathrm{Disc}\,S_{\Gamma_\sigma}(\{k^0_\alpha\},\omega) = is\sum_{\mathrm{F}_\sigma\subset\Gamma_\sigma} 2\pi\delta\left(\sum_{\substack{\text{cut lines}\\ c}} k^0_c - s\omega\right) \\ \times S^+_{\mathrm{F}_\sigma}(\{k^0_\alpha\},\omega)S^-_{\mathrm{F}_\sigma}(\{k^0_\alpha\},\omega),\end{aligned} \tag{3.5}$$

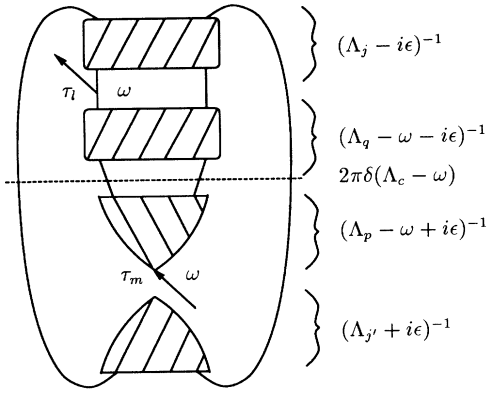


FIG. 6. A schematic illustration of a time-ordered cut diagram $\mathrm{F}_\sigma$ corresponding to the Disc $S_{\Gamma_\sigma}$ in Eq. (3.4a) where the external frequency flows out above the cut. The vertices are chronologically ordered so that the largest time is $\tau_n$ and the smallest $\tau_0$, and $n \geq j \geq l{+}1$, $l \geq q \geq c{+}1$, $c{-}1 \geq p \geq m{+}1$, and $m \geq j' \geq 1$. The dashed line indicates the cut, and the contribution of all the intervals are shown at the right.

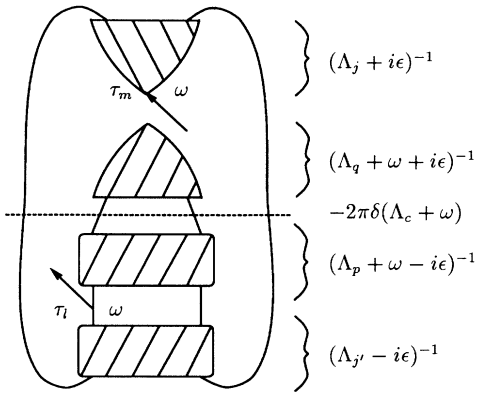


FIG. 7. A schematic illustration of a time-ordered cut diagram $\mathrm{F}_\sigma$ corresponding to the Disc $S_{\Gamma_\sigma}$ in Eq. (3.4b) where the external frequency flows out below the cut. The vertices are chronologically ordered so that the largest time is $\tau_n$ and the smallest $\tau_0$, and $n \geq j \geq m{+}1$, $m \geq q \geq c{+}1$, $c{-}1 \geq p \geq l{+}1$, and $l \geq j' \geq 1$. The dashed line indicates the cut, and the contribution of all the intervals are shown at the right.

where the sum runs over all cut time-ordered diagrams, indicated by $\mathrm{F}_\sigma$, generated by the original time-ordered diagram $\Gamma_\sigma$,

$$S^+_{\mathrm{F}_\sigma}(\{k^0_\alpha\},\omega) \equiv \prod_{p=n-n_++1}^{n} \Big(\Lambda_p - \omega_p - is\epsilon\Big)^{-1} \tag{3.6}$$

denotes the contribution from the upper part of the cut diagram, and

$$S^-_{\mathrm{F}_\sigma}(\{k^0_\alpha\},\omega) \equiv \prod_{p=1}^{n_-} \Big(\Lambda_p - \omega_p + is\epsilon\Big)^{-1} \tag{3.7}$$

denotes the contribution from the lower part. Here $n_+$ is the number of interaction vertices above the cut, $n_-$ is the number of interaction vertices below the cut, and $s$ is $+1$ if the external frequency enters the lower part of the diagram, $-1$ otherwise. $\omega_p$ is the net (real continuous) external frequency flowing out of the vertices above the $p$th interval and equals $s\omega$ for intervals between the external vertices, and 0 otherwise. The contribution of each interval is summarized by the rules.

(1) Each uncut time interval between two vertices contributes a factor which is the inverse of the sum of frequencies of all lines crossing the interval, minus the total external frequency flowing out of the vertices above the interval, plus or minus $i\epsilon$. If the interval is on the side where the external frequency flows out, use $-i\epsilon$, if on the other side, use $+i\epsilon$.

(2) The cut interval contributes $2\pi$ times a delta function whose argument is the sum of the frequencies of all lines crossing the interval minus the external frequency flowing out of the vertex above the cut. The sign of the delta function is $(+)$ if the cut is above the vertex where the external frequency flows in and $(-)$ if below.

The fact that each side of the cut interval contributes the energy denominators with the same sign of $i\epsilon$ is important, and will enable these cut time-ordered diagrams to be resummed into the simpler cut Feynman diagrams considered in the next section. If a different set of $i\epsilon$'s than Eqs. (2.26), (2.42), and (2.43) had been used, the result would have been equivalent but less conveniently organized. Note that if the contribution of an interval $j$ in a cut time-ordered diagram is given by $(\Lambda_j - \omega \pm i\epsilon)^{-1}$, then the contribution of the corresponding interval in the time-reversed diagram is $(\Lambda_j + \omega \pm i\epsilon)^{-1}$. Thus, the contributions from a time ordered diagram and its time reversal are related to each other by an overall sign change combined with the flipping of the external frequency, $\omega \to -\omega$.

Combining these results, the discontinuity of a complete Feynman diagram $\Gamma$ can be expressed as a sum over all possible cuts,

$$\mathrm{Disc}\, C^{(\Gamma)}_{AB}(q) \equiv \sum_{\mathrm{F}\subset\Gamma} \Big(D^{(\mathrm{F})}_{AB}(\mathbf{q},q^0) - D^{(\mathrm{F})}_{AB}(\mathbf{q},-q^0)\Big)\ , \tag{3.8}$$

where the sum runs over all topologically distinct cut Feynman diagrams, denoted by F, and $D^{(\mathrm{F})}_{AB}(\mathbf{q},q^0)$ is the sum of contributions from all topologically equivalent cut time-ordered diagrams with a common cut and with the external frequency flowing out above the cut:

$$D^{(\mathrm{F})}_{AB}(q) = \frac{(-\lambda)^{n-1}}{\mathcal{S}_\Gamma} \int \prod_{L\in\Gamma} \frac{d^3\mathbf{k}_L}{(2\pi)^3} \prod_{\alpha\in\Gamma} \frac{dk^0_\alpha}{2\pi} \Big(1 + n(k^0_\alpha)\Big) \rho(|\mathbf{k}_\alpha|, k^0_\alpha) f_{AB}(\{\mathbf{k}_L\},\mathbf{q})$$
$$\times \left[\sum_{\mathrm{F}_\sigma\subset\mathrm{F}} 2\pi i\delta\left(\sum_{\substack{\text{cut lines}\\ c}} k^0_c - q^0\right) S^+_{\mathrm{F}_\sigma}(\{k^0_\alpha\},q^0)\, S^-_{\mathrm{F}_\sigma}(\{k^0_\alpha\},q^0)\right]\ . \tag{3.9}$$

Obtaining a more compact form of this result is the goal of the next section.

## IV. SIMPLE CUTTING RULES

For diagrams with $n$ vertices, the number of cut time-ordered diagrams is more than $n!$ times greater than the number of original Feynman diagrams. This is obviously inconvenient. Fortunately, one may combine different cut time-ordered diagrams so that each side of the cut yields ordinary Feynman diagrams.

Consider a set of topologically equivalent cut time-ordered diagrams with $n-1$ interaction vertices. This means diagrams with the same connectivity and the same cut, but with any relative ordering of the vertices on each side of the cut. Assume, for convenience, that the external operator $\hat{A}$ emits the external momentum $q$ above the cut. Let $\mathrm{F}$ denote this set of cut time-ordered diagrams (or equivalently, a single cut Feynman diagram). As shown in the last section, the sum of contributions from the graphs in the set $\mathrm{F}$ is given by $D_{AB}^{(\mathrm{F})}(q)$ (3.9). For each choice of the cut interval, the contribution $D_{AB}^{(\mathrm{F})}(q)$ sums up only half of the cut time-ordered diagrams. The remaining cut time-ordered diagrams are those where the external momentum flows out below the cut. These diagrams, as explained in the previous section, sum to $-D_{AB}^{(\mathrm{F})}(\mathbf{q},-q^0)$. Below, it will also be shown that

$$D_{AB}^{(\mathrm{F})}(\mathbf{q},-q^0)=e^{-q^0\beta}\,D_{AB}^{(\mathrm{F})}(\mathbf{q},q^0)\;. \tag{4.1}$$

Consequently, the spectral density $\rho_{AB}(q)$ has the diagrammatic expansion

$$i\rho_{AB}(q)=\sum_{\mathrm{F}}(1-e^{-q^0\beta})\,D_{AB}^{(\mathrm{F})}(q)\;, \tag{4.2}$$

where the sum runs over all topologically distinct cut diagrams $\mathrm{F}$.

We wish to rewrite the expression for $D_{AB}^{(\mathrm{F})}(q)$ in Eq. (3.9) as a product of two contributions representing each half of the cut diagram, with each contribution produced by the standard Feynman rules. This will generate a finite temperature generalization of the zero temperature Cutkosky rules. To proceed, note that the cut separates the vertices of the diagram into two disjoint sets, the upper part and lower part. Thus the summation over time orderings, with the cut fixed, can be separated into two independent summations over permutations of vertices on each side of the cut. Therefore, the total contribution from a cut diagram $\mathrm{F}$ can be written as

$$D_{AB}^{(\mathrm{F})}(q)=\frac{i}{\mathcal{S}_\Gamma}\int\frac{d^4q'}{(2\pi)^4}\prod_{\substack{\text{cut lines}\\ c}}\left(\frac{d^4k_c}{(2\pi)^4}\left(1+n(k_c^0)\right)\rho(k_c)\right)D_A^{\Gamma^+}(\{k_c\},q)\,D_B^{\Gamma^-}(\{k_c\},q')\;, \tag{4.3}$$

where $D_A^{\Gamma^+}(\{k_c\},q)$ and $D_B^{\Gamma^-}(\{k_c\},q')$ denote the results of resummation in the upper ($\Gamma^+$) and the lower ($\Gamma^-$) parts of the cut diagram, respectively. Here and henceforth the subscript $c$ labels the different cut lines. An extra integration over $q'$ is introduced because each factor $D_{\mathcal{O}^\pm}^{\Gamma^\pm}$ (with $\mathcal{O}^+\equiv\hat{A}$ and $\mathcal{O}^-\equiv\hat{B}$) will contain an overall four-momentum-conserving $\delta$ function. Hence their product will produce an overall factor of $(2\pi)^4\delta^4(q-q')$ which is removed by the integration over $q'$.

Explicitly, the contributions from each half of the diagram are given by

$$D_{\mathcal{O}^\pm}^{\Gamma^\pm}(\{k_c\},q)\equiv(-\lambda)^{n_\pm}(2\pi)^3\delta^3\left(\sum_c\mathbf{k}_c-\mathbf{q}\right)\int\prod_{L\in\Gamma^\pm}\frac{d^3\mathbf{k}_L}{(2\pi)^3}\prod_{\alpha\in\Gamma^\pm}\frac{dk_\alpha^0}{2\pi}\left(1+n(k_\alpha^0)\right)\rho(|\mathbf{k}_\alpha|,k_\alpha^0)$$
$$\times f_{\mathcal{O}^\pm}(\{\mathbf{k}_L\},\mathbf{q})\,\mathcal{J}^\pm(\{k_\alpha^0\},\{k_c^0\},q^0)\;. \tag{4.4}$$

The factor $f_{\mathcal{O}^\pm}(\{\mathbf{k}_L\},\mathbf{q})$ represents the action of a single external operator. The factors $\mathcal{J}^\pm(\{k_\alpha^0\},\{k_c^0\},q^0)$ denote the sum of the products of the frequency denominators over the permutations of the vertices on each side of the cut:

$$\mathcal{J}^\pm(\{k_\alpha^0\},\{k_c^0\},q^0)$$
$$\equiv 2\pi\delta\left(\sum_c k_c^0-q^0\right)\sum_{\mathrm{F}_\sigma\subset\Gamma^\pm}S_{\mathrm{F}_\sigma}^\pm(\{k_\alpha^0\},\{k_c^0\},q^0)\;, \tag{4.5}$$

where, as before,

$$S_{\mathrm{F}_\sigma}^+(\{k_\alpha^0\},\{k_c^0\},\omega)\equiv\prod_{j=n-n_++1}^{n}\left(\Lambda_j-\omega_j-i\epsilon\right)^{-1}\;, \tag{4.6}$$

and

$$S_{\mathrm{F}_\sigma}^-(\{k_\alpha^0\},\{k_c^0\},\omega)\equiv\prod_{j=1}^{n_-}\left(\Lambda_j-\omega_j+i\epsilon\right)^{-1}\;. \tag{4.7}$$

Here it should be understood that the summation is over the permutations of vertices on each side of the cut. Recall that the times are labeled in chronological order so that the largest time is always labeled as $\tau_n$ for each time ordering. Thus, in any given time ordering, $\Lambda_j-\omega_j$ can be replaced by $\Omega_j^n=\sum_{s=j}^n\sigma_s$ [cf. Eq. (2.20)].

For the upper part of the diagram, the product of frequency denominators in $S_{\mathrm{F}_\sigma}^+$, Eq. (4.6), together with the overall frequency-conserving delta function, has exactly the same form as the contribution of a zero temperature time-ordered diagram corresponding to the upper part of the cut diagram. Consequently, $S_{\mathrm{F}_\sigma}^+(\{k_\alpha^0\},\{k_c^0\},q^0)$ times a delta function equals the ordered real-time integral,

$$2\pi\delta(\Omega^n_{n-n_+})\, S^+_{\mathrm{F}_\sigma}(\{k^0_\alpha\},\{k^0_c\},q^0)$$

$$= (i)^{n_+}\int_{-\infty}^{\infty} dt_{n-n_+}\, e^{-i\sigma_{n-n_+}t_{n-n_+}}\int_{t_{n-n_+}}^{\infty} dt_{n-n_++1}\, e^{-i\sigma_{n-n_++1}t_{n-n_++1}}\cdots\int_{t_{n-1}}^{\infty} dt_n\, e^{-i\sigma_n t_n}\ , \quad (4.8)$$

which is simply the $t_n \geq t_{n-1} \geq \cdots \geq t_{n-n_+}$ piece of the unordered real-time integral:

$$\mathcal{J}^+(q^0,\{k^0_\alpha\},\{k^0_c\}) = (i)^{n_+}\int_{-\infty}^{\infty}\prod_{p=n-n_+}^{n} dt_p\, e^{iq^0 t_l}\prod_{\substack{\text{cut lines}\\ c}} e^{-ik^0_c t_d}\prod_{\substack{\text{uncut lines}\\ \alpha}} e^{-i(k^0_\alpha - i\epsilon)|t_a - t_b|} \quad (4.9)$$

corresponding to the same half of the cut diagram. As done previously, $t_l$ denotes the vertex time where the external frequency $q^0$ flows out and all the times $\{t_a, t_b, t_d, t_l\}$ are within the set $\{t_{n-n_+},\ldots,t_n\}$. The frequencies of the cut lines are regarded as flowing into the upper part of the diagram; hence each cut line contributes a factor of $e^{-ik^0_c t_d}$, while the external line contributes a factor of $e^{iq^0 t_l}$. The equality of the sum (4.5) and the unordered time integral (4.9) can be easily established since the unordered integral $\mathcal{J}^+(q^0,\{k^0_\alpha\},\{k^0_c\})$ precisely generates the sum of contributions from all orderings of vertices above the cut. For future use we note that changing the integration variables $\{t_p\}$ to $\{-t_p\}$ shows that

$$\mathcal{J}^+(q^0,\{k^0_\alpha\},\{k^0_c\}) = \mathcal{J}^+(-q^0,\{k^0_\alpha\},\{-k^0_c\})\ . \quad (4.10)$$

Thus, for both $\mathcal{J}^+(\{k^0_\alpha\},\{k^0_c\},q^0)$ and $D^{\Gamma^+}_{\mathcal{O}^+}(\{k_c\},q^0)$, changing the sign of the external frequency is equivalent to changing the sign of the frequencies of all cut lines. This fact will be needed to prove the relation (4.1).

The complete contribution $D^{\Gamma^+}_{\mathcal{O}^+}(\{k_c\},q)$ of the upper half of the cut diagram can thus be produced by applying standard Feynman rules using the simple real-time propagator

$$G(|\mathbf{k}|,|t-t'|) = \int\frac{d\omega}{2\pi}\Big(1+n(\omega)\Big)\rho(|\mathbf{k}|,\omega)e^{-i\omega|t-t'|}\ , \quad (4.11)$$

or equivalently, using its Fourier transform

$$\begin{aligned}\tilde{G}(k) &\equiv \int dt\, e^{ik^0 t}G(|\mathbf{k}|,|t|)\\ &= \int\frac{d\omega}{2\pi i}\Big(1+n(\omega)\Big)\left(\frac{1}{k^0+\omega-i\epsilon}-\frac{1}{k^0-\omega+i\epsilon}\right)\rho(|\mathbf{k}|,\omega)\\ &= \int\frac{d\omega}{2\pi}\Big(1+n(\omega)\Big)\left(\frac{2i\omega}{(k^0)^2-(\omega-i\epsilon)^2}\right)\rho(|\mathbf{k}|,\omega)\end{aligned} \quad (4.12)$$

for each uncut line, and regarding each cut line as an external line with definite frequency and momentum. Explicitly, this result is

$$D^{\Gamma^+}_{\mathcal{O}^+}(\{k_c\},q) = (-i\lambda)^{n_+}(2\pi)^4\delta^4\left(\sum_c k_c - q\right)\int\prod_{L\in\Gamma^+}\frac{d^4k_L}{(2\pi)^4}\, f_{\mathcal{O}^+}(\{\mathbf{k}_L\},\mathbf{q})\prod_{\alpha\in\Gamma^+}\tilde{G}(k_\alpha)\ . \quad (4.13)$$

The same procedure may be applied to the lower part of the cut diagram. Because of the difference in sign of the infinitesimal imaginary parts, the result involves complex conjugated propagators. Noting that $\Omega^n_j = -\Omega^{j-1}_0$, the contribution of a particular time-ordering $\tau_{n_-} \geq \tau_{n_--1} \geq \cdots \geq \tau_1 \geq 0$ can be expressed by the real-time integral

$$2\pi\delta(\Omega^{n_-}_0)S^-_{\mathrm{F}_\sigma}(\{k^0_\alpha\},\{k^0_c\},q^0) = (-i)^{n_-}\int_{\infty}^{\infty} dt_{n_-}\, e^{i\sigma_{n_-}t_{n_-}}\int_{-\infty}^{t_{n_-}} dt_{n_--1}\, e^{i\sigma_{n_--1}t_{n_--1}}\cdots\int_{-\infty}^{t_1} dt_0\, e^{i\sigma_0 t_0}\ . \quad (4.14)$$

As before, summing over all time orderings of the vertices below the cut produces

$$\mathcal{J}^-(q^0,\{k^0_\alpha\},\{k^0_c\}) = (-i)^{n_-}\int_{-\infty}^{\infty}\prod_{q=0}^{n_-} dt_q\, e^{-iq^0 t_m}\prod_{\substack{\text{cut lines}\\ c}} e^{ik^0_c t_g}\prod_{\substack{\text{uncut lines}\\ \alpha}} e^{i(k^0_\alpha+i\epsilon)|t_e-t_f|}\ , \quad (4.15)$$

where in going from (4.14) to (4.15) the integration variables $\{t_q\}$ are changed to $\{-t_q\}$. The time $t_m$ denotes the vertex where the external frequency $q^0$ flows in and the times $\{t_e,t_f,t_g,t_m\}$ are now within the set $\{t_0,\ldots,t_{n_-}\}$.

The factors in $\mathcal{J}^-(q^0,\{k_\alpha^0\},\{k_c^0\})$ are complex conjugated compared to those in $\mathcal{J}^+(q^0,\{k_\alpha^0\},\{k_c^0\})$. Thus, the complete contribution from the lower part of the cut diagram is produced by applying standard Feynman rules, but using complex conjugated propagators. Once again, both $\mathcal{J}^-(q^0,\{k_\alpha^0\},\{k_c^0\})$ and $D_{\mathcal{O}^-}^{\Gamma^-}(\{k_c\},q)$ are invariant under simultaneous changes in sign of $q^0$ and the cut frequencies. The final contribution of the lower part is

$$D_{\mathcal{O}^-}^{\Gamma^-}(\{k_c\},q)=(i\lambda)^{n_-}(2\pi)^4\delta^4\left(\sum_c k_c-q\right)\int\prod_{L\in\Gamma^-}\frac{d^4k_L}{(2\pi)^4}\,f_{\mathcal{O}^-}(\{\mathbf{k}_L\},\mathbf{q})\prod_{\alpha'\in\Gamma^-}\tilde{G}(k_{\alpha'})^*\,. \tag{4.16}$$

Combining both halves, the complete expression for the finite temperature cut diagram, defined as the sum of all topologically equivalent cut time-ordered diagrams with the cut corresponding to $2\pi\delta(\sum_c k_c^0-q^0)$, is given by

$$D_{AB}^{(\mathrm{F})}(q)=\frac{i(-i\lambda)^{n_+}(i\lambda)^{n_-}}{\mathcal{S}_\Gamma}\int\prod_{L\in\Gamma}\frac{d^4k_L}{(2\pi)^4}\prod_{\substack{\text{cut lines}\\ c}}\left(1+n(k_c^0)\right)\rho(k_c)f_{AB}(\{\mathbf{k}_L\},\mathbf{q})\prod_{\alpha\in\Gamma^+}\tilde{G}(k_\alpha)\prod_{\alpha'\in\Gamma^-}\tilde{G}(k_{\alpha'})^*\,, \tag{4.17}$$

using the fact that after integrating over the delta functions the remaining cut momenta are all independent loop momenta. This expression for the finite temperature cut diagrams is almost identical to that of zero temperature cut diagrams given by the Cutkosky rules. The cut may be regarded as dividing a diagram into shaded and unshaded regions. The unshaded region is above the cut where the external operator $\hat{A}$ emits the external momentum $q$. An uncut line with the four-momentum $k$ in the unshaded region represents the propagator $\tilde{G}(k)$. An uncut line with four-momentum $p$ in the shaded region represents the complex conjugated propagator $\tilde{G}(p)^*$. A cut line with four-momentum $q$ flowing into the unshaded region represents the phase-space factor $[1+n(q^0)]\rho(q)$.

Once again, note that only cut time-ordered diagrams with the external momentum flowing out above the cut enter the definition of the finite temperature cut diagram. The sum of the remaining cut time-ordered diagrams where the external momentum flows out below the cut are not independent and can be expressed in terms of the same finite temperature cut diagrams. As stated earlier, the sum of cut time-ordered diagrams where the external momentum flows out below the cut equals

$$-D_{AB}^{(\mathrm{F})}(\mathbf{q},-q^0)=\frac{-i}{\mathcal{S}_\Gamma}\int\frac{d^4q'}{(2\pi)^4}\prod_{\substack{\text{cut lines}\\ c}}\left(\frac{d^4k_c}{(2\pi)^4}\left(1+n(k_c^0)\right)\rho(k_c)\right)D_A^{\Gamma^+}(\{k_c\},(\mathbf{q},-q^0))\,D_B^{\Gamma^-}(\{k_c\},(\mathbf{q}',-q'^0))\,. \tag{4.18}$$

Both of the factors $D_{\mathcal{O}^\pm}^{\Gamma^\pm}$ are invariant under simultaneous sign changes of both the external frequency and the frequencies of the cut lines. Thus, changing the integration variables $\{k_c^0\}$ to $\{-k_c^0\}$ easily yields

$$D_{AB}^{(\mathrm{F})}(\mathbf{q},-q^0)=e^{-q^0\beta}\,D_{AB}^{(\mathrm{F})}(\mathbf{q},q^0)\,, \tag{4.19}$$

after using the relation $[1+n(-k^0)]\rho(|\mathbf{k}|,-k^0)=e^{-k^0\beta}[1+n(k^0)]\rho(|\mathbf{k}|,k^0)$ and overall frequency conservation.

The relations (4.19) and (4.2) combined with the standard relation [1,13],

$$\rho_{AB}(q)=(1-e^{-q^0\beta})\,\sigma_{AB}(q)\,, \tag{4.20}$$

show that the finite temperature cut diagrams $D_{AB}^{(\mathrm{F})}(q)$ directly generate the perturbative expansion of the correlation function:[5]

$$\begin{aligned} i\sigma_{AB}(q)&\equiv i\int dx\,e^{-iqx}\langle\hat{A}(x)\hat{B}(0)\rangle\\ &=\sum_{\mathrm{F}}D_{AB}^{(\mathrm{F})}(q)\,. \end{aligned} \tag{4.21}$$

Furthermore, the definition of the spectral density as a commutator, or

$$\rho_{AB}(q)=\sigma_{AB}(q)-\sigma_{BA}(-q)\,, \tag{4.22}$$

combined with the identity (4.20), implies that the sum of all cut time-ordered diagrams with the external momentum $q$ flowing out below the cut yields $-\sigma_{BA}(-q)$. Thus $\sigma_{BA}(-q)$ can be interpreted as the sum of all finite temperature cut diagrams where the external operator $\hat{A}$ emits the momentum $q$ from the *shaded* region whereas $\sigma_{AB}(q)$ is given by cut diagrams where operator $\hat{A}$ is in the *unshaded* region.

Finite temperature cut diagrams differ from zero temperature cut diagrams in one notable way. At zero temperature, each side of a cut diagram must itself be a connected diagram. But at nonzero temperature, the cut

[5]Results equivalent to Eqs. (4.13), (4.16), (4.18), (4.21) can be extracted from Refs. [6,8].

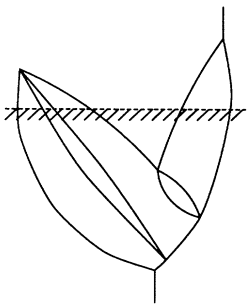

FIG. 8. A typical finite temperature cut diagram which is absent at zero temperature. The shaded line separates the shaded and unshaded region.

need only separate the two external vertices.[6] Although the complete diagram must be connected, each half of the cut diagram, considered separately, may have multiple disconnected parts. A typical such diagram is illustrated in Fig. 8. This change reflects the fact that at nonzero temperature, a perturbation can lower the internal energy of the original thermal ensemble. At the diagrammatic level, this means that a cut line can have a four-momentum with either positive or negative energy, and so a collection of physical excitations can have vanishing net four-momentum. Consequently, a disconnected piece in half of a cut diagram can produce a nonzero "on-shell" result at finite temperature.

Given the previous results, the diagrammatic rules for the spectral density can be cited in two equivalent ways. One may use finite temperature cut diagrams to calculate the correlation function $\sigma_{AB}(q)$ and then simply multiply it by $(1-e^{-q^0\beta})$ to obtain the spectral density. Or, one may use finite temperature cut diagrams to calculate both $\sigma_{AB}(q)$ and $\sigma_{BA}(-q)$ separately and subtract them to yield the spectral density. The following diagrammatic rules summarize the latter approach which directly reflects the commutator origin of the spectral density. Rules for the first method are obtained simply by restricting the set of diagrams to those in which the external momentum flows out of the unshaded region of the cut diagram. These rules also apply when the external operators involve time derivatives of the elementary fields. A sketch of the proof is contained in Appendix B. To calculate the perturbative expansion of a finite temperature spectral density we must do the following.

(1) Draw all suitable topologically distinct cut diagrams (including a choice of shading). Label each line with a four-momentum $k$, assign the external four-momentum, and conserve four-momentum at each vertex.

(2) On the unshaded side of the cut, apply the standard Feynman rules; use the propagator $\tilde{G}(k)$ [cf. Eq. (4.12)] for each uncut line and assign a factor of $-i\lambda$ to each interaction vertex.

(3) On the shaded side, apply complex conjugated Feynman rules; use the propagator $\tilde{G}(k)^*$ for each uncut line, and assign $i\lambda$ to each interaction vertex.

(4) Each cut line with momentum $k$ flowing from the shaded region into the unshaded region contributes a thermal phase space factor

$$\tilde{\Delta}(k) \equiv \left(1+n(k^0)\right)\rho(k) .$$

(5) Integrate over all loop momenta, and divide by the symmetry factor. If the external frequency flows out of the shaded region, assign an additional factor of $-1$.

As the temperature goes to zero, the phase space factor $\tilde{\Delta}(k)$ develops a step function $\theta(k^0)\,\rho(k)|_{T=0}$ which forces all cut lines to carry positive energy. Inserting the spectral density of the bare propagator reduces $\tilde{\Delta}(k_c)$ to $\theta(k_c^0)\delta(k_c^2+m^2)$ and immediately reduces these finite temperature rules to the standard zero temperature Cutkosky rules.

## V. APPLICATIONS

To illustrate the application of the cutting rules, consider the spectral density of the correlation function $\langle[\hat{\phi}^2(\mathbf{x},t),\hat{\phi}^2(0)]\rangle$ in the $\lambda\phi^4$ theory. In particular, we will focus on the quantity

$$\eta_{\phi^2\phi^2} \equiv \lim_{\omega\to 0}\lim_{\mathbf{k}\to 0}\left[\frac{\rho_{\phi^2\phi^2}(\mathbf{k},\omega)}{\omega}\right] . \tag{5.1}$$

This differs from the shear viscosity (1.2) only by the omission of spatial derivatives in the operator insertions. Including these derivatives would make only minor notational changes in the following discussion. When the Boltzmann equation is valid, the transport coefficients can be shown to be inversely proportional to the scattering cross section. Finite-order perturbative calculations of the transport coefficient can never produce that result, and hence a partial resummation of diagrams from all orders will always be necessary. The example discussed here will show similar behavior.

We will consider the first few terms in the expansion of $\rho_{\phi^2\phi^2}$ and analyze the resulting low momentum behavior. The cutting rules will be used to evaluate cut diagrams where the external momentum $q$ flows out of the unshaded region. Multiplying the result with $(1-e^{-q^0\beta})$ will yield the complete contribution to the spectral density, as discussed in the previous section.

The first contribution to the spectral density comes from the one-loop cut diagram in Fig. 9. Following the rules given in Sec. IV, the cut lines contribute factors of $[1+n(k^0)]\rho(|\mathbf{k}|,k^0)$ and $[1+n(-k^0+\omega)]\rho(|\mathbf{k}|,-k^0+\omega)$ where $\rho(|\mathbf{k}|,k^0)$ is the full one-particle spectral density and the spatial external momentum is set to 0. Multiplying these contributions by a factor of $(1-e^{-\beta\omega})$ yields

[6]Thus, for each diagram with a total of $n$ interaction vertices, the number of finite temperature cut diagrams (neglecting symmetry factors) is $2^n$. The separation of vertices into the shaded and the unshaded regions of the cut diagram is completely equivalent to the language of the circled and the uncircled vertices used in Ref. [6].

$$\rho^{1\text{ loop}}_{\phi^2\phi^2}(0,\omega) = 2(1-e^{-\beta\omega})\int \frac{d^4k}{(2\pi)^4}\Big(1+n(-k^0+\omega)\Big)\Big(1+n(k^0)\Big)\rho(|\mathbf{k}|,-k^0+\omega)\rho(|\mathbf{k}|,k^0)\ . \tag{5.2}$$

(The first factor of 2 is an overall symmetry factor.) For a free theory, the one-particle spectral density $\rho(k)$ reduces to a $\delta$ function,

$$\rho_{\text{free}}(|\mathbf{k}|,k^0) = \frac{k^0}{|k^0|}2\pi\delta(k^2+m^2)\ , \tag{5.3}$$

and the resulting integral (5.2) agrees with the standard result [18]. The $\delta$ function in the free one-particle spectral density $\rho_{\text{free}}(|\mathbf{k}|,k^0)$ requires that $k^0 = \pm E_k$, and $\rho_{\text{free}}(|\mathbf{k}|,-k^0+\omega)$ requires $k^0 = \pm E_k+\omega$. When $|\omega|$ is less than twice the mass $m$, these two conditions cannot be satisfied simultaneously, and hence $\eta^{\text{free}}_{\phi^2\phi^2} = \lim_{\omega\to 0}\rho^{\text{free}}_{\phi^2\phi^2}(0,\omega)/\omega$ vanishes in a massive free theory.[7]

This result changes dramatically when the spectral density has finite width. If

$$\Sigma(|\mathbf{k}|,i\nu) \equiv \tilde{G}^E(|\mathbf{k}|,i\nu)^{-1} - \nu^2 - (\mathbf{k}^2+m^2) \tag{5.4}$$

denotes the full self-energy, then one-particle spectral density is

$$\rho(k) = \frac{-2\Sigma^I(k)}{[k^2+m^2+\Sigma^R(k)]^2+[\Sigma^I(k)]^2}\ , \tag{5.5}$$

where $\Sigma(k) \equiv \Sigma^R(k)+i\Sigma^I(k)$ when $k^0$ approaches the real line from above in the complex $k^0$ plane. The spectral density has a peak at $k^0 = E_k$ where the single particle energy $E_k$ is the solution to $E_k^2 = \mathbf{k}^2+m^2+\Sigma^R(\mathbf{k},E_k)$. The width of the peak is given by $\Gamma_k \equiv -\Sigma^I(\mathbf{k},E_k)/2E_k$, and for weak coupling this width is $O(\lambda^2)$ (since the first graph which contributes an imaginary part is the two-loop graph in Fig. 10). For sufficiently small coupling, the frequency variation in the self-energy is negligible over the width of the peak in the spectral density. Hence the single-particle spectral density may be approximated by

$$\rho(k) \approx \frac{4k^0\Gamma_k}{[(k^0)^2-E_k^2]^2+4(k^0\Gamma_k)^2}\ . \tag{5.6}$$

With a finite-width single-particle spectral density, the integrand in Eq. (5.2) is smooth for all $\omega$, and the limit $\omega\to 0$ and the momentum integral may be freely interchanged. Hence

$$\begin{aligned}\eta^{1\text{ loop}}_{\phi^2\phi^2} &\equiv \lim_{\omega\to 0}\frac{\rho^{1\text{ loop}}_{\phi^2\phi^2}(0,\omega)}{\omega} = 2\beta\int\frac{d^4k}{(2\pi)^4}\,n(k^0)\Big(1+n(k^0)\Big)\Big(\rho(|\mathbf{k}|,k^0)\Big)^2\\ &\approx 2\beta\int\frac{d^3\mathbf{k}}{(2\pi)^3}\int\frac{dk^0}{2\pi}n(k^0)\Big(1+n(k^0)\Big)\left(\frac{4k^0\Gamma_k}{[(k^0)^2-E_k^2]^2+4(k^0\Gamma_k)^2}\right)^2\\ &= \beta\int\frac{d^3\mathbf{k}}{(2\pi)^3}\,n(E_k)\Big(1+n(E_k)\Big)\frac{1}{E_k^2\Gamma_k}\Big(1+O(\Gamma_k/E_k)\Big)\ ,\end{aligned} \tag{5.7}$$

where the prefactor $\beta$ comes from $\lim_{\omega\to 0}[(1-e^{-\beta\omega})/\omega]$. Since the width $\Gamma_k$ is $O(\lambda^2)$ for weak coupling, this approximation to $\eta^{1\text{ loop}}_{\phi^2\phi^2}$ diverges in the weak coupling limit. This is in accord with the earlier expectation based on the Boltzmann equation.

The evaluation of the leading contribution to $\eta^{1\text{ loop}}_{\phi^2\phi^2}$ is now reduced to the evaluation of the width $\Gamma_k$. The cutting rules can be used to evaluate the width since the imaginary part of the self-energy is proportional to the discontinuity in this case. The self-energy diagram with the least number of interaction vertices is shown in Fig. 10. Using the result of the previous section, the contribution from this diagram is given by

$$\begin{aligned}\Sigma^I_{2\text{ loop}}(q) = -\frac{\lambda^2}{12}(1-e^{-\beta q^0})\int\frac{d^4k_1}{(2\pi)^4}\int\frac{d^4k_2}{(2\pi)^4}\Big(1+n(k_1^0)\Big)\rho(k_1)\\ \times\Big(1+n(k_2^0)\Big)\rho(k_2)\Big(1+n(q^0-k_1^0-k_2^0)\Big)\rho(q-k_1-k_2)\ .\end{aligned} \tag{5.8}$$

[7] In the massless limit, the one-loop spectral density $\rho^{\text{free}}_{\phi^2\phi^2}(0,\omega)$ in the free theory is nonzero and can easily be calculated explicitly. One finds

$$\begin{aligned}\lim_{m\to 0}\rho^{\text{free}}_{\phi^2\phi^2}(0,\omega) &= 2(1-e^{-\beta\omega})\int\frac{d^4k}{(2\pi)^4}\,\frac{1}{4|\mathbf{k}|^2}\Big(1+n(k^0)\Big)\Big(1+n(-k^0+\omega)\Big)\\ &\quad\times\Big(2\pi\delta(k^0-|\mathbf{k}|)-2\pi\delta(k^0+|\mathbf{k}|)\Big)\Big(2\pi\delta(-k^0+\omega-|\mathbf{k}|)-2\pi\delta(-k^0+\omega+|\mathbf{k}|)\Big)\\ &= \frac{1}{4\pi}\coth(\beta\omega/4)\ .\end{aligned}$$

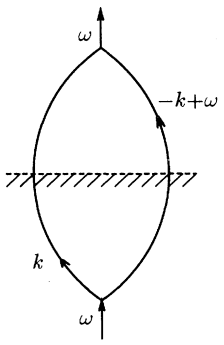


FIG. 9. The lowest order diagram for the spectral density of $\langle[\hat{\phi}^2(\mathbf{x},t),\hat{\phi}^2(0)]\rangle$ at zero external three-momentum.

The overall factor of 12 comes from the symmetry factor of 6 and a factor of 2 difference between the discontinuity and the imaginary part. This two-loop diagram is the first single-particle irreducible self-energy diagram in the skeleton expansion. To evaluate Eq. (5.8), some approximation to the full single-particle self-energy $\Sigma(q)$ must be made.

One may easily show that approximating the full spectral density by the free single-particle spectral density is adequate to yield the leading result. An approximation scheme using dressed propagators is equivalent to adding a self-energy term $\frac{1}{2}\phi\Sigma\phi$ to the free Lagrangian and subtracting from the interaction term:

$$-\mathcal{L}=\frac{1}{2}\phi(-\partial_\tau^2-\nabla^2+m^2+\Sigma)\phi+\left(\frac{1}{4!}\lambda\phi^4-\frac{1}{2}\phi\Sigma\phi\right)\ . \tag{5.9}$$

By using $[\nu^2+\mathbf{k}^2+m^2+\Sigma(i\nu,\mathbf{k})]^{-1}$ as the basic propagator and treating $-\frac{1}{2}\phi\Sigma\phi$ as an additional interaction, a rearranged perturbation series can be obtained for any physical quantity. If $\Sigma$ is the exact self-energy, then this expansion is what was previously called the skeleton expansion. Since the propagator already contains the full self-energy, all corrections to the propagator must add up to zero in the skeleton expansion. Thus, the sum of contributions from all one-particle irreducible skeleton self-energy diagrams minus the contribution from the additional interaction $\Sigma$ vanishes. This is one of the standard Dyson equations for the $\lambda\phi^4$ theory.

If in the Lagrangian (5.9) one adds and subtracts only the lowest order, the sum of contributions from all single-particle irreducible self-energy diagrams minus the contribution of the additional interaction $\Sigma$ will be nonzero, but it will be of higher order than the lowest-order self-energy. In the resulting expansion, the lowest-order self-energy acts as an infrared cutoff and renders finite higher-order on-shell single-particle reducible diagrams which would normally have been divergent. Provided that the correct $O(\lambda^2)$ single-particle width appears in the rearranged propagators, the resulting diagrammatic series will generate corrections suppressed by positive powers of the interaction strength $\lambda$ (perhaps modified by logarithms). Thus, it is sufficient to compute the leading behavior of (the imaginary part of) the two-loop self-energy diagram by replacing the single-particle spectral densities by free spectral densities in the weak coupling limit. The actual calculation is somewhat complicated [19,20]. Here we exhibit only the leading result at high temperature ($T\gg m$) and vanishing spatial momentum, $q=(m,0)$. One finds [21]

$$\Sigma_{2\ \mathrm{loop}}^{I}(m,0)=-\mathrm{sgn}(m)\frac{\lambda^2T^2}{768\pi}\Big(1+O((m/T)\ln(T/m))\Big) \tag{5.10}$$

and the static one-particle width is given by

$$\Gamma_{(m,0)}=-\Sigma^I(m,0)/2m=\lambda^2T^2/1536m\pi(1+O(\lambda))\ . \tag{5.11}$$

Using this result, the leading behavior of $\eta_{\phi^2\phi^2}^{1\ \mathrm{loop}}$ in the high temperature limit can be found:

$$\begin{aligned}\eta_{\phi^2\phi^2}^{1\ \mathrm{loop}}&=\beta\int\frac{d^3\mathbf{k}}{(2\pi)^3}\,n(E_k)\Big(1+n(E_k)\Big)\frac{1}{E_k^2\Gamma_k}\\&\quad\times\Big(1+O(\Gamma_k/E_k)\Big)\\&=\frac{768}{\lambda^2T\pi}\ln(aT/m)\left(1+O(m/T,\lambda^2)\right)\ .\end{aligned} \tag{5.12}$$

The numerical constant $a$ in the logarithm depends on the spatial momentum dependence of the width $\Gamma_k$. (For a constant width, $a=2$ [20].) The appearance of the logarithm reflects the fact that when $m$=0 this integral is logarithmically divergent. However, even a massless field develops a finite thermal mass at finite temperature. In the case of massless high temperature $\lambda\phi^4$ theory, the one-loop self-energy provides a thermal mass $m_T=(\lambda/24)^{\frac{1}{2}}T$ [14,21].

The one-loop result $\eta_{\phi^2\phi^2}^{1\ \mathrm{loop}}$ is not the only relevant contribution to $\eta_{\phi^2\phi^2}$ at this order. There are other diagrams with more interaction vertices that also make contribution of the same order as the one-loop result. This is because there are additional infrared divergences at finite temperature, and the infrared cutoffs provided by the thermal scattering width of the self-energy contribute negative powers of $\lambda$. For example, consider the "eye" diagram shown in Fig. 11. Since this is closely related to the two-loop vertex correction, we will denote it by $\rho^v_{\phi^2\phi^2}(0,\omega)$. Applying the cutting rules, the graph in Fig. 11 together with the one with all internal lines reversed generates the contribution

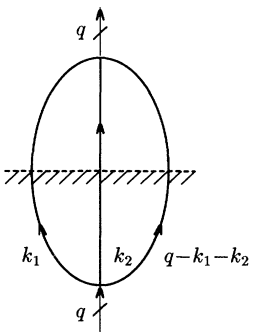


FIG. 10. A two-loop self-energy diagram in $\lambda\phi^4$ theory. The slashed lines are the amputated external lines.

$$\rho^{v}_{\phi^2\phi^2}(0,\omega) = (1-e^{-\beta\omega})\,\lambda^2 \int \frac{d^4k_1}{(2\pi)^4}\frac{d^4k_2}{(2\pi)^4}\frac{d^4k_3}{(2\pi)^4} \int \frac{d\omega_1}{2\pi}\frac{d\omega_2}{2\pi}\Big(1+n(-k_1^0-k_2^0-k_3^0+\omega)\Big)$$
$$\times\Big(1+n(k_1^0)\Big)\Big(1+n(\omega_1)\Big)\Big(1+n(k_2^0)\Big)\Big(1+n(\omega_2)\Big)\Big(1+n(k_3^0)\Big)$$
$$\times\rho(|\mathbf{k}_1|,k_1^0)\,\rho(|\mathbf{k}_1|,\omega_1)\,\rho(|\mathbf{k}_2|,k_2^0)\,\rho(|\mathbf{k}_2|,\omega_2)$$
$$\times\rho(|\mathbf{k}_3|,k_3^0)\,\rho(|-\mathbf{k}_1-\mathbf{k}_2-\mathbf{k}_3|,-k_1^0-k_2^0-k_3^0+\omega)$$
$$\times\left(\frac{2i\omega_1}{(-k_1^0+\omega)^2-(\omega_1-i\epsilon)^2}\frac{2i\omega_2}{(-k_2^0+\omega)^2-(\omega_2-i\epsilon)^2}\right). \quad (5.13)$$

If free one-particle spectral densities are used, the kinematical constraints require $|\omega_1|=|k_1^0|=E_{k_1}$, and $|\omega_2|=|k_2^0|=E_{k_2}$. Under these constraints, the contribution of the uncut lines in the lower frequency limit becomes

$$\frac{2i\omega_1}{(-k_1^0+\omega)^2-(\omega_1-i\epsilon)^2}\frac{2i\omega_2}{(-k_2^0+\omega)^2-(\omega_2-i\epsilon)^2}$$
$$=-\frac{1}{\omega^2}\frac{\omega_1\omega_2}{k_1^0k_2^0}\,. \quad (5.14)$$

Combined with the $(1-e^{-\beta\omega})$ prefactor, this will cause $\rho^{v}_{\phi^2\phi^2}(0,\omega)$ to diverge linearly as $\omega\to 0$.

The nonzero width of finite temperature one-particle spectral densities will cut off this divergence. The two uncut propagators will be almost on shell. To estimate the contributions of this diagram, these propagators may be replaced by their maximum on-shell values, $\sim 1/E_k\Gamma_k$. Thus as the external frequency $\omega$ tends to 0, the diagram's leading contribution behaves as $\omega\lambda^2/\Gamma_{k_1}\Gamma_{k_2}\sim\omega/\lambda^2$, effectively replacing the $\omega^2$ denominator in Eq. (5.14) by the product of inverse lifetimes $\Gamma_{k_1}\Gamma_{k_2}$. [As before, the factor of $\omega$ comes from the small $\omega$ limit of the prefactor $(1-e^{-\beta\omega})$.] Note that this contribution is the same order in $\lambda$ as the leading one-loop result. This demonstrates that the one-loop calculation is not sufficient to obtain the correct weak coupling, low frequency behavior. We will show below that there are an infinite number of diagrams contributing at the same order in the zero frequency limit.

The leading behavior of the contribution of a general diagram in the limit of zero external four-momentum is not difficult to determine. Since the source of the inverse powers of the coupling is the infrared cutoff provided by the thermal scattering width of the self-energy, the weak coupling behavior is directly related to the infrared singularity of the diagram when all the lines are interpreted as free propagators. At zero temperature, there is a standard argument that asserts that the appearance of on-shell singularities is due either to the pinching of an integration contour by coalescing poles or to poles colliding with the end point of a contour [22]. A similar argument may be given for the diagrams considered here. Suppose we approximate the one-particle spectral density by the Lorentzian form

$$\rho(k)\sim\frac{1}{E_k}\left(\frac{\Gamma}{(k^0-E_k)^2+\Gamma^2}-\frac{\Gamma}{(k^0+E_k)^2+\Gamma^2}\right). \quad (5.15)$$

In this approximation, both $\tilde{G}(|\mathbf{k}|,k^0)$ and $\rho(|\mathbf{k}|,k^0)$ contain four simple poles in the complex $k^0$ plane at $E_k\pm i\Gamma$ and $-E_k\pm i\Gamma$. Thus the products of propagators and spectral densities $\tilde{G}(|\mathbf{k}|,k^0)\tilde{G}(|\mathbf{k}|,k^0+\omega)$, $\rho(|\mathbf{k}|,k^0)\tilde{G}(|\mathbf{k}|,k^0+\omega)$, and $\rho(|\mathbf{k}|,k^0)\rho(|\mathbf{k}|,k^0+\omega)$ all have poles within a circle of radius $\Gamma$ as $\omega\to 0$ which approach the contour from opposite sides. Therefore, after performing the frequency integrations, a loop containing one of these products will behave as $\sim 1/\Gamma$ as $\omega\to 0$. All one has to do to determine the leading behavior as $\omega\to 0$

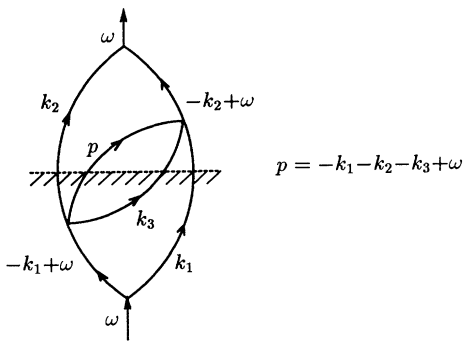


FIG. 11. A cut "vertex correction" diagram contributing to the spectral density of $\langle[\hat{\phi}^2(\mathbf{x},t),\hat{\phi}^2(0)]\rangle$ at zero external three-momentum. The dashed line indicates the cut. The contribution of this diagram together with the one with all internal lines reversed is denoted by $\rho^{v}_{\phi^2\phi^2}(0,\omega)$.

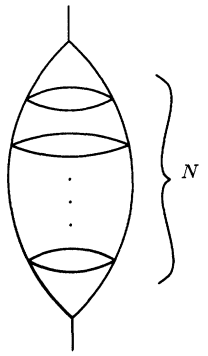


FIG. 12. The planar ladder diagram with $N$ rungs in $\lambda\phi^4$ theory.

is then to count the number of such loops in skeleton expansion diagrams.

As an example, consider a generalization of the diagram in Fig. 11 to the $(2N+1)$-loop planar "ladder" diagram illustrated in Fig. 12. When the external four-momentum vanishes, there are $N+1$ pairs of lines with identical four-momentum in this diagram. Equivalently, there are $N+1$ loops each of which behave like $1/\Gamma$. Thus, all cut diagrams for the $(2N+1)$-loop planar ladder diagram in Fig. 12 can generate $O(\omega\lambda^{2N}/\Gamma^{N+1})$ contributions in the low frequency limit. [As always, a factor of $\omega$ comes from the prefactor $(1-e^{-\beta\omega})$.] Since the single-particle width is order $\lambda^2$, all planar graphs of this form contribute at order $\omega/\lambda^2$ regardless of the number of loops. (Similar behavior may be found in other processes [14].) Other $(2N+1)$-loop graphs with crossed loops (nonplanar graphs) are necessarily of higher order because they cannot have as many pairs of lines sharing the same four-momentum.[8] Summing all leading contributions is a nontrivial problem. We hope to pursue this matter in a future paper.

## ACKNOWLEDGMENTS

The constant encouragement and guidance of L. G. Yaffe and L. S. Brown are greatly appreciated.

## APPENDIX A: *CPT* INVARIANCE AND THE SPECTRAL DENSITY

Consider the consequence of the *CPT* invariance on the spectral density of the two-point function of any pair of operators $\hat{A}$ and $\hat{B}$. Assume that $\hat{A}$ and $\hat{B}$ have definite behavior under a *CPT* transformation:

$$\hat{\Theta}\hat{A}^\dagger(\mathbf{x},t)\hat{\Theta}^{-1}=\eta_A\hat{A}(-\mathbf{x},-t) \tag{A1}$$

and

$$\hat{\Theta}\hat{B}^\dagger(\mathbf{x},t)\hat{\Theta}^{-1}=\eta_B\hat{B}(-\mathbf{x},-t) \tag{A2}$$

where $\hat{\Theta}$ is the antiunitary *CPT* operator and $|\eta_A|=|\eta_B|=1$. If the equilibrium density matrix $\hat{\rho}\equiv e^{-\beta\hat{H}}/\mathrm{Tr}\,e^{-\beta\hat{H}}$ of the theory is *CPT* invariant (i.e., no chemical potential), then the following identities hold:

$$\begin{aligned}\langle[\hat{A}(\mathbf{x},t),\hat{B}(0)]\rangle^* &= \sum_n\langle\hat{\Theta}n|\hat{\Theta}\hat{\rho}[\hat{A}(\mathbf{x},t),\hat{B}(0)]\hat{\Theta}^{-1}\hat{\Theta}|n\rangle\\ &= \eta_A\eta_B\sum_{n'}\langle n'|\hat{\rho}[\hat{A}^\dagger(-\mathbf{x},-t),\hat{B}^\dagger(0)]|n'\rangle\\ &= -\eta_A\eta_B\sum_{n'}\langle n'|\hat{\rho}[\hat{B}^\dagger(\mathbf{x},t),\hat{A}^\dagger(0)]|n'\rangle\\ &= -\eta_A\eta_B\langle[\hat{B}^\dagger(\mathbf{x},t),\hat{A}^\dagger(0)]\rangle\ .\end{aligned} \tag{A3}$$

Hermiticity implies the independent relation

$$\begin{aligned}\langle[\hat{A}(\mathbf{x},t),\hat{B}(0)]\rangle^* &= \langle[\hat{B}^\dagger(0),\hat{A}^\dagger(\mathbf{x},t)]\rangle\\ &= \langle[\hat{B}^\dagger(-\mathbf{x},-t),\hat{A}^\dagger(0)]\rangle\ .\end{aligned} \tag{A4}$$

In terms of the Fourier transforms, the relation (A3) reads $\rho^*_{AB}(\mathbf{k},\omega)=-\eta_A\eta_B\rho_{B^\dagger A^\dagger}(-\mathbf{k},-\omega)$, and Eq. (A4) gives $\rho^*_{AB}(\mathbf{k},\omega)=\rho_{B^\dagger A^\dagger}(\mathbf{k},\omega)$. Combined, these imply that

$$-\eta_A\eta_B\,\rho_{B^\dagger A^\dagger}(-\mathbf{k},-\omega)=\rho_{B^\dagger A^\dagger}(\mathbf{k},\omega)\ . \tag{A5}$$

If $\hat{B}=\hat{A}^\dagger$, then, the Hermiticity relation (A4) gives $\rho^*_{AA^\dagger}(\mathbf{k},\omega)=\rho_{AA^\dagger}(\mathbf{k},\omega)$ implying that $\rho_{AA^\dagger}(\mathbf{k},\omega)$ is real. Since space is isotropic, the spectral density must also be an even function of the spatial momentum $\mathbf{k}$. Thus in any *CPT*-invariant equilibrium state the spectral density $\rho_{AA^\dagger}(|\mathbf{k}|,\omega)$ is an odd function of frequency,

$$\rho_{AA^\dagger}(|\mathbf{k}|,\omega)=-\rho_{AA^\dagger}(|\mathbf{k}|,-\omega)\ . \tag{A6}$$

## APPENDIX B: OPERATORS WITH TIME DERIVATIVES

If the external operators involve time derivatives, the sum over the permutations of the vertices in the upper part of a cut diagram is

$$\mathcal{J}^+_A(q^0,\{k^0_\alpha\},\{k^0_c\})=(i)^{n_+}\int_{-\infty}^{\infty}\prod_{p=n-n_+}^{n}dt_p\,e^{iq^0t_l}\prod_{\substack{\text{cut lines}\\ c}}e^{-ik^0_ct_d}\hat{O}_A(d/dt_l)\prod_{\substack{\text{uncut lines}\\ \alpha}}e^{-i(k^0_\alpha-i\epsilon)|t_b-t_a|}\ , \tag{B1}$$

where $\hat{O}_A(d/dt_l)$ is the action of the external operator $\hat{A}$. The spatial momentum dependence of $\hat{O}_A(d/dt_l)$ is suppressed here since it is of no importance in this discussion. As in the main text, $t_l$ denotes the vertex time where the external frequency $q^0$ flows out and all the times $\{t_a,t_b,t_d,t_l\}$ are within the set $\{t_{n-n_+},\ldots,t_n\}$.

If the time orderings are all reversed, then the same (now lower) parts of the diagram sum to

$$\begin{aligned}\mathcal{J}^+_A(q^0,\{k^0_\alpha\},\{-k^0_c\}) &= (i)^{n_+}\int_{-\infty}^{\infty}\prod_{p=n-n_+}^{n}dt_p\,e^{-iq^0t_l}\prod_{\substack{\text{cut lines}\\ c}}e^{-ik^0_ct_d}\hat{O}_A(-d/dt_l)\prod_{\substack{\text{uncut lines}\\ \alpha}}e^{-i(k^0_\alpha-i\epsilon)|t_b-t_a|}\\ &= (i)^{n_+}\int_{-\infty}^{\infty}\prod_{p=n-n_+}^{n}dt_p\,e^{iq^0t_l}\prod_{\substack{\text{cut lines}\\ c}}e^{ik^0_ct_d}\hat{O}_A(d/dt_l)\prod_{\substack{\text{uncut lines}\\ \alpha}}e^{-i(k^0_\alpha-i\epsilon)|t_b-t_a|}\ .\end{aligned} \tag{B2}$$

[8]Strictly speaking, this applies only when the mass is nonzero. If the mass is zero, the statistical factors can provide additional sources of divergent behavior.

In the first equality, the sign change of $q^0$ to $-q^0$ comes from the change in sign of the frequency denominators. The sign change of the derivative $d/dt_l$ comes from the fact that the factor of frequency brought down by the time derivative must change sign when the time ordering is reversed. Since the factors corresponding to the uncut lines $e^{-i(k_\alpha^0 - i\epsilon)|t_b - t_a|}$ are not changed, the sign of the derivative $d/dt_l$ must change. The final equality comes from changing the integration variables $\{t_p\}$ to $\{-t_p\}$.

A similar argument holds for the other half of the diagram. Thus the whole expression for the sum of all cut time-ordered diagrams with the external momentum flowing out below the cut is the same as the expression with external momentum flowing out above the cut except for changing the sign of the frequencies of all cut lines. Changing the sign of the cut frequencies introduces additional exponential factors coming from the statistical factors. Using the overall frequency conservation, those factors combine to yield $e^{-q^0\beta}$.

## APPENDIX C: NONZERO CHEMICAL POTENTIAL

Consider a complex scalar field theory with nonzero chemical potential $\mu$ associated with the conserved charge. The Euclidean Lagrange density for this theory is given by

$$-\mathcal{L} = \phi^*(-\partial_\tau^2 - \nabla^2 + m^2 - \mu^2)\phi + \frac{\lambda}{3!}(\phi^*\phi)^2 + i\mu(\phi^*\partial_\tau\phi - \phi\partial_\tau\phi^*) \,. \tag{C1}$$

One may regard the theory as having two different free propagators:

$$\tilde{G}_\mu^E(|\mathbf{k}|, i\nu) \equiv \int d^3\mathbf{x} \int_0^\beta d\tau\, e^{-i\mathbf{k}\cdot\mathbf{x} + i\nu\tau} \langle \mathcal{T}(\hat{\phi}^*(\mathbf{x}, -i\tau)\hat{\phi}(0))\rangle_0 = \frac{1}{E_k^2 + (\nu - i\mu)^2} \tag{C2}$$

and

$$\tilde{G}_{-\mu}^E(|\mathbf{k}|, i\nu) \equiv \int d^3\mathbf{x} \int_0^\beta d\tau\, e^{-i\mathbf{k}\cdot\mathbf{x} + i\nu\tau} \langle \mathcal{T}(\hat{\phi}(\mathbf{x}, -i\tau)\hat{\phi}^*(0))\rangle_0 = \frac{1}{E_k^2 + (\nu + i\mu)^2} \,, \tag{C3}$$

where $\langle\cdots\rangle_0$ indicates the average is taken with only the quadratic part of the Lagrangian. Because of this difference, each line in a Feynman diagram is assigned a direction which indicates which end of the line corresponds to $\hat{\phi}^*$, or equivalently the direction of the flow of conserved charge. At each interaction vertex, two lines must point outwards while the other two point inwards. In coordinate space, a line pointing to $(\tau_b, \mathbf{x}_b)$ from $(\tau_a, \mathbf{x}_a)$ corresponds to the propagator $\langle \mathcal{T}(\hat{\phi}^*(\mathbf{x}_b, -i\tau_b)\hat{\phi}(\mathbf{x}_a, -i\tau_a))\rangle_0$, or in momentum space, if momentum is assigned in accordance with the arrow, then each line represents the propagator $\tilde{G}_\mu^E(|\mathbf{k}_\alpha|, i\nu_\alpha)$. There is then no need to introduce $\tilde{G}_{-\mu}^E(|\mathbf{k}_\alpha|, i\nu_\alpha)$.

The $CPT$ invariance of the system is explicitly broken by the chemical potential term. Nevertheless, an argument similar to the one given in Appendix A can be applied using the relation

$$\hat{\Theta}\hat{\rho}\hat{\Theta}^{-1} = \hat{\Theta}\frac{e^{-\beta\hat{H} + \mu\hat{Q}}}{\mathrm{Tr}e^{-\beta\hat{H} + \mu\hat{Q}}}\hat{\Theta}^{-1} = \frac{e^{-\beta\hat{H} - \mu\hat{Q}}}{\mathrm{Tr}e^{-\beta\hat{H} - \mu\hat{Q}}} \,. \tag{C4}$$

The one-particle spectral density is not an odd function of frequency but satisfies

$$\rho_\mu(|\mathbf{k}|, \omega) \equiv -i\,\mathrm{Disc}\,\tilde{G}_\mu(|\mathbf{k}|, \omega) = -\rho_{-\mu}(|\mathbf{k}|, -\omega) \,. \tag{C5}$$

Here $\tilde{G}_\mu(|\mathbf{k}|, i\nu)$ is the fully dressed single-particle propagator in the imaginary-time formalism. The "mixed" propagator is then given by

$$\tilde{G}_\mu(|\mathbf{k}|, \tau) = \int_{-\infty}^{\infty} \frac{d\omega}{2\pi} \Big(\rho_\mu(|\mathbf{k}|, \omega)\,\theta(\tau) + \rho_{-\mu}(|\mathbf{k}|, \omega)\,\theta(-\tau)\Big) e^{-\omega|\tau|} \Big(1 + n(\omega)\Big) \,. \tag{C6}$$

As in the main text, consider a Feynman diagram with a total of $n+1$ vertices. Using the mixed propagators, the contribution of a line with a momentum $\mathbf{k}_\alpha$ pointing to a time $\tau_b$ from time $\tau_a$ is $\tilde{G}_\mu(|\mathbf{k}_\alpha|, \tau_b - \tau_a)$. To evaluate the resulting time integral, one of the times is again set to zero, and the integrand is split into $n!$ terms according to the relative time orderings of remaining $n$ time variables. A typical time integral still is

$$\mathcal{I}(\{k_\alpha^0\}, i\nu) \equiv \int_0^\beta d\tau_n \cdots \int_0^{\tau_3} d\tau_2 \int_0^{\tau_2} d\tau_1 \,\exp\Big\{\sum_{l=1}^n -\sigma_l\tau_l\Big\} \,, \tag{C7}$$

as in Eq. (2.12). Which combination of $\rho_\mu(|\mathbf{k}_\alpha|, k_\alpha^0)$ and $\rho_{-\mu}(|\mathbf{k}_\alpha|, k_\alpha^0)$ multiplies this time integral depends on the particular time ordering that gives rise to the integral. To determine this, draw the corresponding time-ordered diagram with the directions of the arrows determined by the flow of charge. If the arrow of a line $\alpha$ points upwards, it corresponds to a factor of $[1 + n(k_\alpha^0)]\,\rho_\mu(|\mathbf{k}_\alpha|, k_\alpha^0)$, and if it points downwards, then it corresponds to $[1 + n(k_\alpha^0)]\,\rho_{-\mu}(|\mathbf{k}_\alpha|, k_\alpha^0)$.

The time integrations of Eq. (C7) produce

$$\mathcal{I}(\{k_\alpha^0\}, i\nu) = \lim_{\epsilon\to 0} \sum_{k=0}^{n} \left( \prod_{j=1}^{k} (\Omega_j^k - i\epsilon_j^k) \prod_{j'=k+1}^{n} (-\Omega_{k+1}^{j'} + i\epsilon_{k+1}^{j'}) \right)^{-1} \exp\left\{\beta(-\Omega_{k+1}^n + i\epsilon_{k+1}^n)\right\} , \tag{C8}$$

with the same notation used in the main text. Once again, the factor $e^{-\beta \mathrm{Re}\,\Omega_{k+1}^n}$ may be omitted if, at the same time, the sign of all frequencies in the set $\Lambda_{\rm in}^{k+1,n}$, and the sign of the chemical potentials associated with the lines in this set, are also changed. The resulting factors of $\Lambda_j^k$ have the same interpretation as the sum of the frequencies of all lines crossing the interval between $\tau_j$ and $\tau_{j-1}$ when the time ordering is $\tau_k \geq \tau_{k-1} \geq \cdots \geq \tau_j \geq \cdots \geq 0 \geq \tau_n \geq \tau_{n-1} \geq \cdots \geq \tau_{k+1}$. This time ordering is achieved by moving the sequence of times $\tau_n \geq \tau_{n-1} \geq \cdots \geq \tau_{k+1}$ down below zero. Diagrammatically, the only arrows that change directions under this operation are those of the lines in the set $\Lambda_{\rm in}^{k+1,n}$, or equivalently the lines whose chemical potentials had their sign flipped. Thus, it remains true that every upward arrow is assigned to a factor $\rho_\mu$ and a downward arrow to every factor of $\rho_{-\mu}$. As before, the contribution of all time-ordered diagrams is expressed in terms of statistical factors, spectral densities and energy denominators. The process of extracting the spectral density is not affected by the presence of the nonzero chemical potential. The previous discussion in the main text applies without change. The resummation of the cut time-ordered diagrams is possible in terms of a real-time propagator:

$$\begin{aligned}\tilde{G}_\mu(k) &\equiv \int dt\, e^{ik^0 t} \int \frac{d\omega}{2\pi} \Big(\rho_\mu(|\mathbf{k}|,\omega)\,\theta(\tau) + \rho_{-\mu}(|\mathbf{k}|,\omega)\,\theta(-\tau)\Big) e^{-i\omega|t|} \Big(1 + n(\omega)\Big) \\ &= \int \frac{d\omega}{2\pi i} \Big(1 + n(\omega)\Big) \left( \frac{\rho_\mu(|\mathbf{k}|,\omega)}{\omega - k^0 - i\epsilon} + \frac{\rho_{-\mu}(|\mathbf{k}|,\omega)}{\omega + k^0 - i\epsilon} \right) .\end{aligned} \tag{C9}$$

The resulting diagrammatic rules are as follows.

(1) Draw all suitable topologically distinct cut diagrams with directed lines.

(2) Label each line with a four-momentum $k_\alpha$ flowing in the direction of the arrow. Assign external four-momentum where the operators are inserted. Conserve four-momentum at each vertex.

(3) On the unshaded side of the cut, use the standard Feynman rules; assign $\tilde{G}_\mu(k_\alpha)$ to each uncut line $\alpha$, and assign $-i\lambda$ to each interaction vertex.

(4) On the shaded side, use the complex conjugated Feynman rules; assign $\tilde{G}_\mu(k_\alpha)^*$ to each uncut line $\alpha$, and assign $i\lambda$ to each interaction vertex.

(5) To each cut line that points towards the unshaded region, assign

$$\tilde{\Delta}_+(k) \equiv \Big(1 + n(k^0)\Big)\rho_\mu(|\mathbf{k}|, k^0) .$$

To each cut line which points towards the shaded region, assign

$$\tilde{\Delta}_-(k) \equiv n(k^0)\rho_{-\mu}(|\mathbf{k}|, k^0) .$$

(6) Integrate over all loop momenta, and divide by the symmetry factor. If the external frequency flows out of the shaded region, assign an additional factor of $-1$.


[1] For example, see A.L. Fetter and J.D. Walecka, *Quantum Theory of Many Particle Systems* (McGraw-Hill, New York, 1971).

[2] A. Hosoya, M. Sakagami, and M. Takao, Ann. Phys. (N.Y.) **154**, 229 (1984), and references therein.

[3] R. Horsley and W. Schoenmaker, Nucl. Phys. **B280**, 716 (1987).

[4] For example, see G.D. Mahan, *Many-Particle Physics* (Plenum, New York, 1981).

[5] R.L. Kobes and G.W. Semenoff, Nucl. Phys. **B260**, 714 (1985); **B272**, 329 (1986).

[6] R. Kobes, Phys. Rev. D **43**, 1269 (1991), and references therein.

[7] N. Ashida, H. Nakkagawa, A. Niegawa, and H. Yokota, Ann. Phys. (N.Y.) **215**, 315 (1992).

[8] T.S. Evans, Nucl. Phys. **B374**, 340 (1992), and references therein.

[9] M.A. van Eijck and Ch.G. van Weert, Phys. Lett. B **278**, 305 (1992).

[10] G. Baym and A.M. Sessler, Phys. Rev. **131**, 2345 (1963).

[11] A.J. Niemi and G.W. Semenoff, Ann. Phys. (N.Y.) **152**, 105 (1984), and references therein.

[12] G. Baym and N.D. Mermin, J. Math. Phys. **2**, 232 (1961).

[13] For example, see L.S. Brown, *Quantum Field Theory* (Cambridge University Press, Cambridge, England, 1992).

[14] For example, see J.I. Kapusta, *Finite Temperature Field Theory* (Cambridge University Press, Cambridge, England, 1989), and references therein.
[15] R.D. Pisarski, Nucl. Phys. **B309**, 476 (1988).
[16] For example, see J.M. Ziman, *Elements of Advanced Quantum Theory* (Cambridge University Press, Cambridge, England, 1969).
[17] R. Kobes, Phys. Rev. D **42**, 562 (1990), and references therein.
[18] H.A. Weldon, Phys. Rev. D **28**, 2007 (1983).
[19] N.P. Landsman and Ch.G. van Weert, Phys. Rep. **145**, 141 (1987).
[20] H.E. Haber and H.A. Weldon, J. Math. Phys. **23**, 1852 (1982).
[21] R.R. Parwani, Phys. Rev. D **45**, 4695 (1992).
[22] S. Coleman and R.E. Norton, Nuovo Cimento **38**, 438 (1965).
[23] F. Guerin, Institut Non Linéaire de Nice Report No. INLN 1992/22, 1992 (unpublished).